TOPICAL REVIEW

Thermal Modeling of Planar Magnetics: Fundamentals, Review and Key Points

REDA BAKRI [1,2], **GAUTIER CORGNE** [1], **AND XAVIER MARGUERON** [1], (Member, IEEE)

[1]L2EP, ULR 2697, Centrale Lille, Arts et Metiers Institute of Technology, Université de Lille, 59000 Lille, France
[2]L2EP, ULR 2697, HESAM Université, 59000 Lille, France

Corresponding author: Reda Bakri (reda.bakri@ensam.eu)

ABSTRACT High-frequency and high-power density converters are essential for many applications such as automotive and more electric aircraft. To improve power density, planar magnetic components are increasingly used in power electronic converters owing to their advantages, such as less high-frequency losses, repeatability, and better thermal performance compared to conventional wound components. Considerable attention has been paid to their electrical performance. However, the thermal aspects are essential for enhancing completely their performance. Currently, there is an increasing interest in these critical aspects of high-density power converters. This paper presents a literature review of studies on the thermal modeling of planar magnetics. The papers were organized according to the model type and analyzed to highlight their merits and limitations. A multicriteria comparison of the studied papers was performed. Moreover, the key points and issues related to the thermal modeling are addressed to guide designers in enhancing the thermal aspects of planar magnetic components.

INDEX TERMS Planar magnetics, high frequency magnetics, thermal modeling, high power density.

I. INTRODUCTION

Magnetic components play a vital role in power conversion. They ensure key functions, such as energy transfer, storage, filtering, voltage adaptation, and galvanic isolation. However, their significant volume exceeded 50% of the total volume of the power converter. Moreover, magnetics can be a source of a considerable amount of power losses [1]. In applications where volume or weight constraints are critical, such as automotive, aeronautics, avionics, and portable equipment, the need to increase power density and efficiency is a major concern for designers [2]. To achieve this goal, it is necessary to increase the frequency and current density. Even if wide band-gap (WBG) semiconductors, such as silicon carbide (SiC) and gallium nitride (GaN), can reach frequencies up to several MHz [3], [4], [5], [6], [7], [8], passive components, in particular magnetics, remain the main limitation of power converter integration.

In this context, planar magnetic components (PMCs) have gained importance because of their electrical and thermal

The associate editor coordinating the review of this manuscript and approving it for publication was Norbert Herencsar .

properties. These components are based on a flattened magnetic core and winding, as shown in Fig.1a, conversely to the conventional magnetic components (Fig.1b).
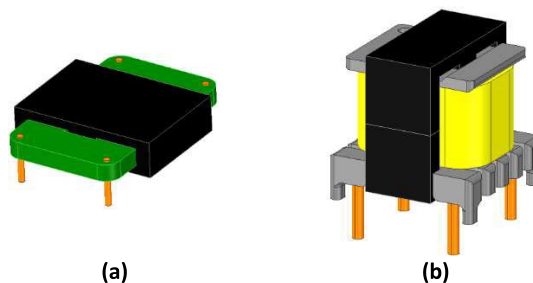

FIGURE 1. High frequency transformer: (a) planar, (b) conventional.

Planar magnetics present many advantages compared to conventional wound components, which make them suitable for high-frequency (HF) and high-power density applications, such as lower HF losses, easier winding interleaving, repeatability, and better thermal performance. owing to their high surface-to-volume ratio. However, PMCs present some limitations, such as a low copper fill factor, limited number

of turns, and higher parasitic capacitances [9], [10]. Planar magnetics is a relatively recent technology for HF magnetics. One of the first papers to introduce PMCs was published by Estrov in 1986 [11]. A literature review of the electrical and electromagnetic aspects of PMCs is presented in [9], [10], and [12].

Most publications have focused on the electrical and electromagnetic aspects to optimize PMC design. However, thermal aspects have been less studied in the literature, even though thermal management and cooling strategies are essential in the design process of PMC. Indeed, the increase in frequency and current density, combined with size reduction, generates strong thermal constraints on the magnetics. To maximize the power density, components often operate near their thermal limits. Consequently, appropriate thermal modeling of PMCs is required to optimize their planar magnetics and improve their thermal performance.

In addition, the temperature had a significant effect on the electrical performance. It affects the physical properties of the various materials composing the PMCs, which impact the loss values and other electrical parameters, such as inductance and capacitance. These effects must be considered in a global study of the power converter performance based on accurate thermal models. The latter can be used to verify the thermal integrity of the PMC and to study the thermal aging linked to the reliability of the component.

To help designers with the thermal modeling of PMCs, this study presents a literature review of different thermal models of planar magnetics. Some key points for the accurate modeling of PMCs were also discussed.

The remainder of this paper is organized as follows. In Section II, the heat transfer fundamentals are presented. In Section III, various PMC thermal models are reviewed, discussed, and compared based on multicriteria. Finally, in the last section, the key points and issues related to the accurate thermal modeling of PMCs are highlighted to establish an effective thermal modeling.

II. THERMAL MODELING FUNDAMENTALS: HEAT TRANSFER MODES

In this section, the heat transfer modes are discussed to understand the basis of the thermal modeling. Heat can flow inside a component or be exchanged with its environment in three heat-transfer modes: conduction, convection, and radiation. These three modes of heat transfer must be considered in thermal modeling to accurately predict the temperature of PMCs.

A. THERMAL CONDUCTION

Thermal conduction is the heat transfer mechanism inside solid and opaque regions, without material deformation, under a temperature gradient. The vibrations of molecules and atoms as well as the movement of free electrons in the material are the origin of this phenomenon.

In the case of an isotropic material with two different temperatures, T_1 and T_2, at its ends (Fig.2), the unidirectional
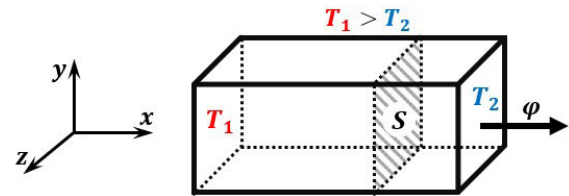

FIGURE 2. Unidimensional thermal conduction.

conduction heat transfer can be expressed by Fourier's law:

$$\varphi = -\lambda \frac{dT}{dx} \tag{1}$$

where T is the temperature in K, φ is the heat flux density in W.m^{-2} and λ is the thermal conductivity in W.K^{-1}. m^{-1}.

Fourier's law can be generalized in three-dimensional:

$$\varphi = -\lambda \, gradT \tag{2}$$

Fourier's law (2) was used to link the power losses (heat generation) of a solid to its temperature field. The heat equation was derived as follows:

$$\rho C_p \frac{\partial T}{\partial t} = q_g + \lambda \Delta T \tag{3}$$

where q_g is the volumetric heat generation in W.m^{-3}, C_p is the specific heat in J.kg^{-1}. K^{-1}, and ρ is the material density in kg.m^{-3}.

Equation (3) is a partial differential equation with a first-order temporal derivative and a second-order spatial derivative. To solve this problem, specifying boundary conditions (BC) in the limit of the studied domain is mandatory. Two types of BC can be used:

- Dirichlet boundary condition where a temperature value is specified.
- Neumann boundary condition, where the temperature derivative is fixed, such that the heat flux leaves the domain (e.g., with convection and radiation).

In the case of a transient study, initial conditions must also be specified.

B. THERMAL CONVECTION

Thermal convection is the heat exchange inside a fluid or between a solid and a fluid owing to fluid movement. Analytical modeling of convection is a difficult task. Such a model requires the resolution of heat transfer equations coupled with fluid mechanical behavior equations.

Empirical Newton's law is often used to model the heat exchange between a solid and a fluid interface (Fig.3):

$$\Phi_{conv} = h_{conv} S (T_s - T_\infty) \tag{4}$$

where ϕ_{conv} is the heat flux due to convection in W, h_{conv} is the convection transfer coefficient in W.m^{-2}°C^{-1}, S is the contact area between solid and fluid in m^2, T_s is the temperature at the fluid surface in °C and T_∞ is the temperature far from the solid surface in °C.
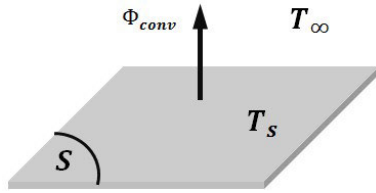
FIGURE 3. Convection heat flux.

If fluid movement is only due to the temperature gradient, the phenomenon is called natural or free convection. If fluid movement is caused by an external force (e.g., pump or fan), it qualifies as forced convection. Table 1 lists the range of convection heat transfer coefficients for air and water in the cases of free and forced convection.

TABLE 1. Convection heat transfer coefficient $Wm^{-2}C^{-1}$.

Material	Natural convection	Forced convection
Air	5-30	100-300
Water	100-1000	300-12000

Many expressions and empirical formulas enable computation of the convection heat-transfer coefficient for several geometrical configurations in free and forced convection. These expressions can be found in most heat transfer engineering resources [13], [14], [15].

C. THERMAL RADIATION
Thermal radiation refers to heat transfer in the form of electromagnetic waves without any contact between the external surface of a body and its thermal environment. Radiation does not require a material medium. Heat transfer by radiation can be described by the Stefan-Boltzmann law for a solid surrounded by a thermal environment (Fig.4), as follows:

$$\Phi_{rad} = \sigma \varepsilon S(T_s^4 - T_\infty^4) \quad (5)$$

where ϕ_{rad} is the heat flux due to convection in W, ε is the surface body emissivity, σ is the Stefan Boltzmann constant $(5.67 10^{-8}$ W.m^{-2}.K$^{-4})$, T$_s$ is the surface temperature in K and T_∞ is the ambient temperature far from the body in K.

For more complex geometries, the heat exchanged by radiation can be computed using the form factors or numerical models [13], [14], [15].

III. THERMAL MODELING OF PLANAR MAGNETIC COMPONENTS: LITERATURE REVIEW
This section presents a review of the relevant literature. The objective was to present an overview of the models employed in scientific publications since the emergence of PMCs. The models were classified into three groups.

- Equivalent thermal resistance
- Thermal resistance network models
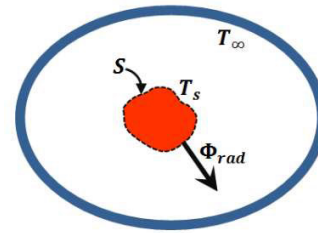- Semi-analytical and numerical models

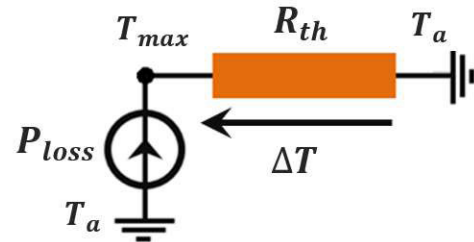**FIGURE 4.** Radiation heat flux.

FIGURE 5. The equivalent circuit of a global thermal resistance model.

In the following sections, the publications are organized according to the thermal modeling types for each group. Their merits and limitations were highlighted before providing a multicriteria-based analysis and global discussion.

A. EQUIVALENT THERMAL RESISTANCE MODELS
The thermal resistance represents the global thermal behavior of a component. This is derived from an analogy with Ohm's law (6), where the temperature rise is linked to power losses (Fig.5):

$$\Delta T = T_{max} - T_a = R_{th} P_{loss} \quad (6)$$

where ΔT is the temperature increase; T_{max} and T_a are the maximal temperature of the component and the ambient temperature, respectively; R_{th} is the thermal resistance; and P_{loss} is the total loss.

The thermal resistance, R_{th} can be obtained from the magnetic component or core manufacturer. It can also be computed from the physical and geometrical properties of components. Analytical formulations are generally based on extensive data fitting using measurements or intensive numerical simulations. Generally, the concept of thermal resistance is very useful and practical, particularly for the early design stage, where a simple and fast calculation of the temperature rise is required. Consequently, equivalent thermal resistance is widely used in the design of HF magnetics. In the following section, some R_{th} models dedicated to PMCs are introduced.

A commonly used expression for computing the thermal resistance of planar magnetic components is given in the Ferroxcube note application (old Philips) [16].

$$R_{th\_Fer} = 24 \cdot V_e^{-0.5} \quad (7)$$

where V_e is the effective volume of the core in cm^3.

A similar expression was used in the Ferroxcube soft ferrite design tool [17] with a difference in the volume

superscript coefficient.

$$R_{th\_Sfd} = 24 \cdot V_e^{-0.54} \qquad (8)$$

In [18], the authors suggested the following expression for the thermal resistance of the magnetic component based on the effective volume of the core:

$$R_{th\_Hur} = \frac{0.06}{\sqrt{V_e \cdot 10^{-6}}} \qquad (9)$$

Another expression (10), which depends only on the component's external area, A_{ext}, expressed in cm^2, was introduced in [19]. It is used in Magnetics Designers software [20] to design magnetic components.

$$R_{th\_Mag} = \frac{1}{14 \cdot A_{ext}} \qquad (10)$$

The main advantage of the presented expressions for thermal resistance [16], [17], [18], [19], [20] is their simplicity; each expression uses only a single parameter, that is, the volume or external area, which can be easily extracted from the manufacturer's datasheets. Despite a lack of information regarding the methods used to derive these expressions and their application conditions, they remain a suitable starting point in the design of PMCs.

Other thermal resistance expressions have been proposed [21], [22], [23] as a function of losses to consider the non-linearity linked to the effect of the component temperature. For example, in [21], the authors suggested an empirical equation to link the power loss, temperature increase, and external area of a component. The equivalent thermal resistance can be derived as follows:

$$R_{th\_Bos}(P_{loss}) = P_{loss}^{-\frac{1}{11}} \left(\frac{0.1}{A_{ext}} \right)^{\frac{1}{1.1}} \qquad (11)$$

Two similar expressions, (12) and (13), were provided in [22] and [23], respectively. Considering the power loss level, the latter allows for greater accuracy in PMCs design, particularly under strong thermal and volume constraints.

$$R_{th\_Mcl}(P_{loss}) = \frac{450}{P_{loss}^{0.174}} \left(\frac{1}{A_{ext} \cdot 10^4} \right)^{0.826} \qquad (12)$$

$$R_{th\_Zha}(P_{loss}) = \frac{1}{P_{loss}^{0.167}} \left(\frac{0.1}{A_{ext}} \right)^{0.833} \qquad (13)$$

To enhance accuracy, in [24], the authors introduced an analytical expression for all sizes of E/PLT (plate) and EE planar cores (14). The particularity of this equation is that the model considers the effect of ambient temperature T_a in the case of natural convection in addition to power losses. An increase in ambient temperature reduced the thermal resistance of the PMCs.

$$R_{th\_Bak}(P_{loss}, T_a) = a_3 P_{loss}^3 + a_2 P_{loss}^2 + a_1 P_{loss} + bT_a + c \qquad (14)$$

where a_3, a_2, a_1, b and c are coefficients given in [24].
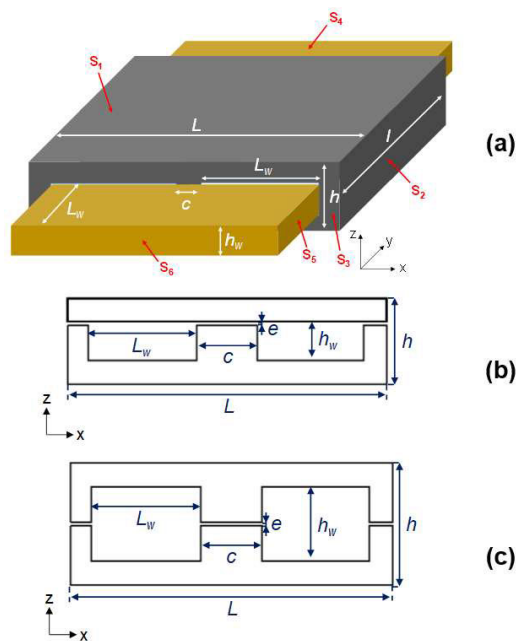

FIGURE 6. Dimensions of planar magnetics under study (a) 3D view, (b) E/PLT core in XZ plane, (c) EE core in XZ plane.

The use of the thermal resistance expressions (7)-(9) requires the core volume value which can be found in the manufacturer datasheet, or can be also computed from the core dimensions. The later are illustrated in a 3D view of a planar component in Fig.6a. Fig.6b and Fig.6c show the dimensions for E/PLT and EE combinations respectively. Table 2 lists the different lengths and the core volume for the standard E/PLT and EE planar cores combinations [17] to allow a fast and straightforward use of thermal resistance formulas.

For expressions (10)-(13), they require the external area of the transformer, including core and winding external areas as illustrated in Fig.6a. This external area can be computed by adding the different external areas of the transformer as expressed in (15) using the transformer dimensions (Fig.6).

$$\begin{aligned} A_{ext} &= 2S_1 + 2S_2 + 2S_3 + 4S_4 + 4S_5 + 2S_6 \\ &= 2Ll + 2hl + 2hL + 8L_w^2 + 4cL_w + 4L_w h_w \end{aligned} \qquad (15)$$

The expression (14) does not require core geometrical parameters, but the coefficients needed for its use are given for every standard core [24].

The eight thermal-resistance models are plotted in Fig.7 as functions of the losses for an E/PLT 38 planar core. Four of the models presented were constant with respect to losses. The other three thermal resistances decreased as power loss increased. The last one varies with the power loss and ambient temperature. The thermal resistance value varies from 20.6 °C/W (R_{th_Hur}) to 12 °C/W (R_{th_Zha}) for 1W losses, whereas for 6W, models give values between 8.9 °C/W (R_{th_Zha}) to 20.6 °C/W (R_{th_Hur}).

TABLE 2. Planar E/PLT and EE core typical lengths, core volume, and component external area [17].

Core	L [mm]	L [mm]	h [mm]	c [mm]	L_w [mm]	h_w [mm]	V_e [cm^3]	A_{ext} [m^2]
E/PLT32	31.75	20.32	9.53	6.35	9.275	3.18	4.560	3325 x 10^{-6}
E/PLT38	38.1	25.4	12.07	7.6	11.315	4.45	8.460	5038 x 10^{-6}
E/PLT43	43.2	27.9	13.6	8.1	13.3	5.4	11.500	6478 x 10^{-6}
E/PLT58	58.4	38.1	14.6	8.1	20.95	6.5	20.800	12003 x 10^{-6}
E/PLT64	64	50.8	15.28	10.2	21.8	5.1	35.500	15147 x 10^{-6}
EE32	31.75	20.32	12.7	6.35	9.275	6.36	53.80	3773 x 10^{-6}
EE38	38.1	25.4	16.52	7.6	11.315	8.9	10.200	5805 x 10^{-6}
EE43	43.2	27.9	19	8.1	13.3	10.8	13.900	7533 x 10^{-6}
EE58	58.4	38.1	21	8.1	20.95	13	24.600	13783 x 10^{-6}
EE64	64	50.8	20.4	10.2	21.8	10.2	40.700	16767 x 10^{-6}
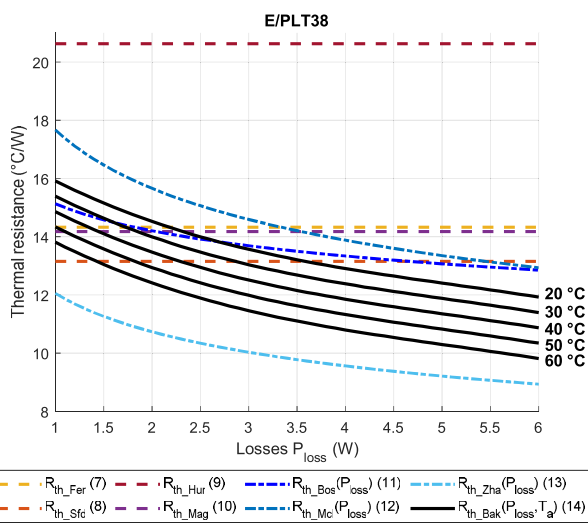
FIGURE 7. Comparison of equivalent thermal resistance models for E/PLT38 planar core.

FIGURE 8. Example of a thermal network with node i connected to three others (j, k, l).

Regarding the difference between the various thermal resistance formulas noticed in Fig.7, the expressions (7)-(13) are based in fitting data. Then, the difference can be explained by the different datasets used in one hand, and the difference between the mathematical description used for the every thermal resistance expression. In addition, the use of two different parameters (volume for (7)-(9) vs external area for (10)-(13)) leads also to some difference in the resulting thermal resistance value. Morever, expressions (11)-(14) consider also power losses as a second parameter to take into account the non-linearities of the thermal resistance.

As an example, for this E/PLT38, the difference between the minimum thermal resistance value and the maximal one leads to 8.6 °C difference for 1W and 70.2 °C for 6W. The range of variation in the models is wide, and consequently, can lead to significant errors in the thermal design of planar magnetics.

Thermal resistance models are very useful for computing the temperature increase in a design procedure; however, they define only one temperature value, which can be the mean or
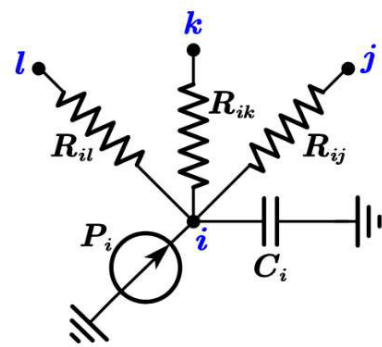
maximal value. To address this problem, more complex analytical models such as lumped-element thermal networks are required. Such a model can provide access to the temperature at several points in a component (e.g., windings, core, and insulator).

B. LUMPED THERMAL NETWORKS
Thermal networks (TN) based on lumped elements are commonly used for thermal modeling in electrical engineering. Indeed, it benefits from the electrical and thermal analogies.

1) INTRODUCTION TO THERMAL NETWORKS
In this type of model, heat conduction is modeled by thermal resistance, heat storage by thermal capacitances, and power losses by current sources. To apply such a model, the component is divided into several elements, where nodes are placed and linked by thermal resistances (Fig.8) and then solved by applying Kirchhoff's laws.

Two types of thermal networks can be defined according to the choice of model elements and nodes:

- Behavioral thermal networks: These refer to the component parts (core and windings), but do not reproduce their physical geometry. Fig.9a shows an example of a planar-component behavioral TN. The windings and core were modeled by two thermal resistances, while

the third resistance was introduced to represent the link between the two parts. This type of model typically contained fewer nodes. In general, the elements were computed from experimental identification.

- Structural or geometrical thermal networks: Node placement and thermal resistance follow the geometry of the component. In Fig.9b, an example of a planar magnetic 2D lumped-element thermal model is shown. One can note A strong link can be observed between the thermal resistance and component geometrical elements. This type of model contains more nodes than behavioral models. It can then provide the temperature values for several points on the component.

Thermal equivalent networks are easy to implement in an electrical circuit software. In the case of a large number of nodes, the problem can be solved using mathematical software in matrix format. The main limitation of the TN is the difficulty in accurately modeling complex geometries. Moreover, there are no fixed rules for setting the number of nodes or splitting components into simple elements.

The TN-reviewed models are classified into three categories: unidimensional (1D); multidimensional TN, which corresponds to structural/geometrical models; and compact TN, which falls into the behavioral TN type.

2) UNIDIMENSIONAL THERMAL NETWORKS

Unidimensional TNs are extensively used in the thermal modeling of PMCs. Indeed, their multilayer structure illustrated in Fig.10a and Fig.10b makes the use of this type of model very suitable.

In the majority of the reviewed papers, every type of layer is represented by a thermal resistor, and losses are injected as a current source in the copper and ferrite layers. Two thermal resistances can be added to represent the

(a)

(b)

FIGURE 9. Thermal networks of planar magnetic components: (a) behavioral, (b) structural/geometrical.

heat exchange with the exterior via thermal convection or radiation (Fig.10c).

One of the first papers dealing with the thermal modeling of PMCs was published by Sayani et al. in 1991 [25]. The authors have suggested thermal and electrical analytical models to design printed circuit board (PCB) transformers called printed sweating board (PWB) transformers. The transformer was designed for a 70 W push-pull converter, working at a frequency of 250 kHz. The component was made of a custom core because commercially available standard planar cores were unavailable. The authors introduced a simple steady-state 1D nodal TN to evaluate temperature increase. This model assumes that the dominant thermal cooling mode is conduction and that the main heat flow path is downward to a heat sink attached to the core bottom. The nodes were placed at the center of each layer and linked by thermal resistance. Finally, the losses are injected as current sources. To validate the model, the transformer windings were excited using DC current without core loss.

Two thermocouples were used to measure the temperatures at the bottom of the core and top of the windings. However, the temperature of the inner layer could not be measured. The model results were in good agreement with the measurements.

A similar model was developed in [26] to compute the temperature of a passive integrated power electronics module by combining all the passive elements in one component.

Linde et al. [27] proposed another 1D thermal model, in which each layer (ferrite, copper, resin, and epoxy insulators) is represented by one thermal resistance. The nodes were placed at the layer interfaces rather than at their centers, as in [25]. These losses were introduced as a current source inserted into the nodes of the copper and ferrite layers. The model was applied to a 200 W planar transformer at 1 MHz based on a modified RM14 core associated with multilayer PCB windings.

Two case studies have been reported: single- and double-sided cooling. These two configurations correspond to a fixed temperature on the top or bottom surface if the component is attached to a heat sink and a zero heat flux in the absence of a heat sink. According to the results of this study, the temperature rise of double-sided cooling was three times lower than that of one-sided cooling.

A 1D thermal model of a 4 kW inductor-capacitance (LC) integrated planar component was studied in [28]. This component was designed to replace the discrete components in the power-resonant converter at a frequency of 100 kHz. The magnetic cores were manufactured by cutting and assembling commercial I-type ferrite cores. As in [27], nodes were placed at the junctions between the layers of the component. The thermal problem was solved in matrix format. The developed model is applied to a planar-component iterative design process. The component was cooled with a heat sink on its bottom face and natural air convection and radiation on its top surface.
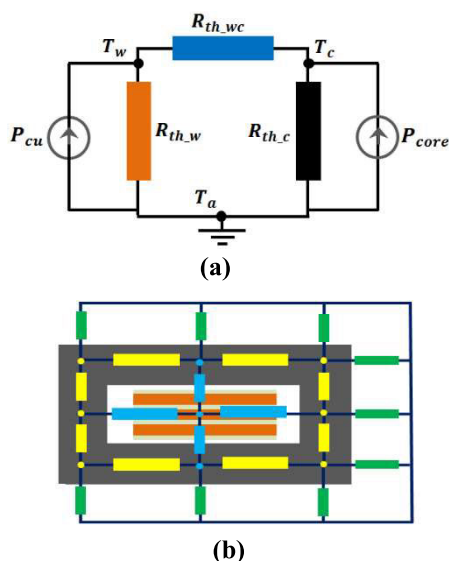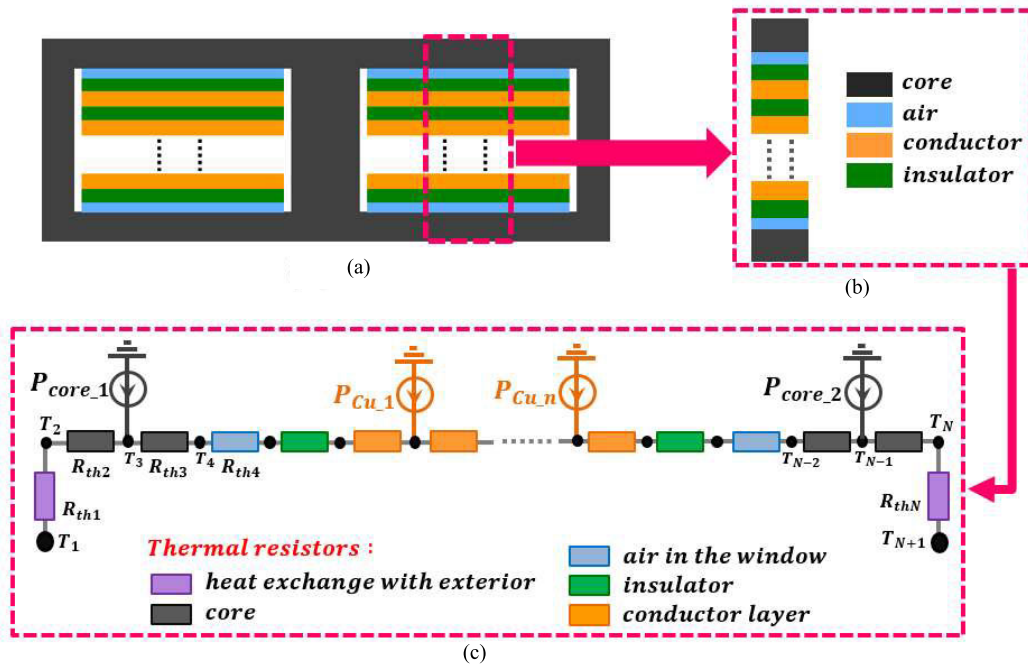
FIGURE 10. Planar magnetic component (a) 2D cut, (b): model's multilayer structure, (c): 1D thermal network.

Another 1D TN of the PMC was proposed in [29]. This model is similar to those presented in [25], [26], [27], and [28]. However, it considers non-linearities introduced by convection and radiation in the external area of the component. The significant contribution of this study is complete 1D modeling, including magnetic and thermal effects. The magnetic model allows loss computation for each layer by using a 1D lumped equivalent magnetic model. For this model, good accuracy was obtained compared with the finite element analysis (FEA) and measurements.

In a more recent paper [30], an electrothermal PMC design was developed. The objective was to optimize a 10 kW planar transformer with a liquid cooler integrated into the windings. A 1D steady-state model is used for the optimization process. The optimization objective was to determine the liquid inlet temperature to limit the core temperature to 100 °C while maximizing the efficiency of the transformer. Two variables were used in this optimization process: the number of turns and the height of the cooler inserted in the core window. Even if the thermal model is not the principal outcome of the study, the cooling system remains original, and the presented solution is very interesting for achieving a compact high-power and high-efficiency PMC.

To improve existing 1D models, Escribano et al. established a unidimensional thermal model for windings [31]. This study aimed to accurately consider the spacing between conductors in existing 1D thermal networks. This spacing can be large compared to that of conductors in planar windings. Thus, it can strongly affect the 1D heat transfer hypothesis owing to the thermal spreading effect, as shown in Fig.11.
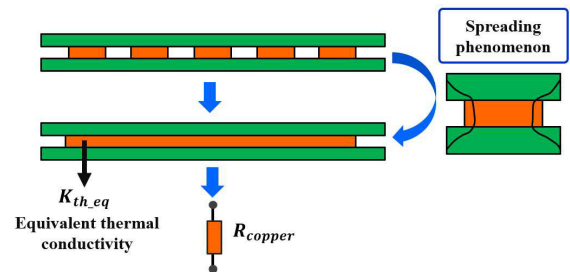

FIGURE 11. Spaced conductors' equivalent 1D thermal resistance as modeld in [31].

Therefore, the multiconductor layer was replaced with a single equivalent layer, represented by a single thermal resistance, considering the spacing effect (Fig.11).

The results of the model were compared with the measurements and 2D FEA results. For this purpose, five test cases of planar transformers with PCB windings with different numbers of layers and conductors were considered. The model showed good agreement with the FEA results and measurements. Although this model can improve the accuracy of 1D models, it cannot overcome other limitations linked to the 3D nature of the heat flow in the entire component.

Steady-state 1D thermal network models introduced in [25], [26], [27], [28], [29], and [30] have the advantage of being fast and straightforward. This can be useful for design purposes. They can also be easily implemented in circuit simulation software, such as PSPICE, PSIM, SABER, and LTSPICE [32], [33], [34], [35]. However, in such a model, the 3D aspect of the component was neglected. Moreover,

the effects of convection and radiation are rarely considered. Therefore, a more detailed and complex thermal network is required.

3) MULTIDIMENSIONAL THERMAL NETWORKS

Multidimensional thermal networks are applied to access the temperature in many parts and locations of the PMCs. For example, to reproduce the 3D shape of a planar transformer, Lewaiter and Ackermann proposed an eight-node thermal resistance network, as illustrated in Fig.12 [36]. The transformer was made of an E-PLT22/16 core with a 4-layer PCB winding. Owing to symmetry, only half of the components were considered for the TN. The model considered half of the PCB winding (Fig.12b), and half of the core (Fig.12c). Eight nodes were allocated as follows: three nodes were placed in the PCB, four on the ferrite core, and one in the gap between the PCB and core. All these nodes were linked by 19 thermal resistances computed analytically from the geometrical and physical properties of the component. The winding was considered homogenous with two effective thermal conductivities: the first was in the direction parallel to the PCB layers, whereas the second was in the normal direction. The model was compared with the FEA results for many case studies based on power dissipation and cooling methods. The heat transfer coefficient value was modified to model different cooling methods. The results were then compared with measurements in the case of natural convection. For the measurements, copper losses were generated by a DC current in the windings and core losses were generated by an additional heating wire around the core. This model has the advantage of reducing the number of nodes, while reproducing the 3D shape of the component. The main reason for this is winding homogenization, which limits the results to the mean winding temperature.

A similar model was used in the design process through optimization in [37]. The results were validated by FEA performed using the COMSOL Multiphysics software [38] and experimental measurements.

A thermal equivalent network that follows the component geometry was established in [39] to investigate the thermal behavior of a planar integrated Inductor Capacitor and Transformer (LCT). The TN was built around four nodes linked with six resistances representing the thermal conduction between the component elements and four thermal resistances to model the heat exchanged by convection and radiation. The formulas used to compute the convection and radiation heat coefficients are described in detail. Two cases were treated: a linear case with a fixed heat exchange coefficient and a non-linear case where heat exchange coefficients depend on temperature. The last case requires iterative calculation. The LTC planar magnetic component was studied in horizontal and vertical positions for various loss values. The model agrees with the measurements for both the linear and non-linear cases. However, the results showed that the linear model was more accurate. This can be explained by the fact that the heat exchange coefficients were fitted from
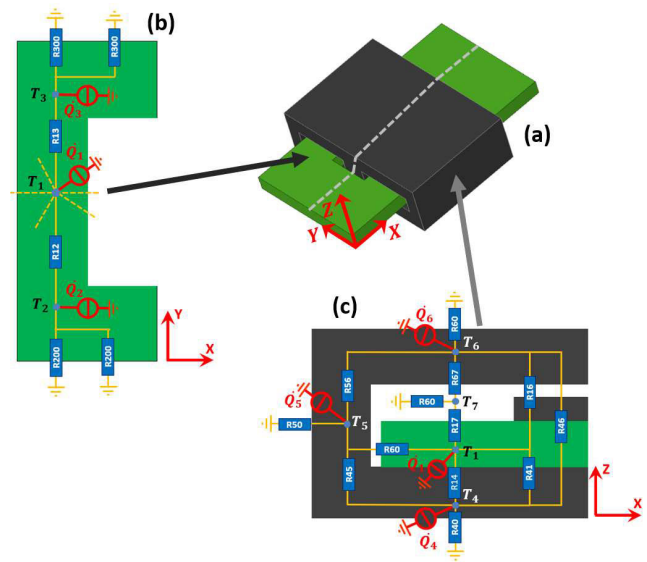

FIGURE 12. Thermal network of planar magnetic component as introduced in [36]: (a) 3D geometry, (b) winding model, (c) 8-nodes core model.

measurements in the linear model, whereas in the non-linear model, they were computed using empirical correlations. The proposed model has a reduced number of nodes and can consider the non-linearity of the boundary conditions (i.e., convection and radiation) that depend on the external surface temperatures. Such a model can be interesting for design or optimization processes; however, it requires more nodes and good knowledge of the heat exchange with the environment to increase its accuracy.

Shafaei et al. introduced, in [40], a 3D frequency-dependent thermal model. Only a quarter of the transformer was considered because of its symmetry. The 3D lumped element model contained 15 nodes, as shown in fig.13. The part under the core is presented using a 2D thermal network. 4 three-dimensional thermal resistances were added to the core. Every winding layer was modeled by two parallel resistances to complete the 3D aspect of the component. Finally, three frequency-dependent thermal resistances were added to consider the frequency effect on thermal behavior. Finally, to complete the model, convection and radiation thermal resistances were added to the external area to model the heat exchange with the ambient, while losses were injected into the nodes placed in the core and winding copper layers.

The values of these thermal resistances were computed analytically from the component frequency and physical and geometrical properties. According to, the thermal surface resistance decreases with frequency and can significantly affect the temperature of the component. This model was applied to study the transient temperatures of two planar transformers designed for an LLC converter with a resonance frequency of 200 kHz. The two transformers were cooled using a heat sink attached to the bottom of the core and natural convection on the remaining external surfaces. To validate
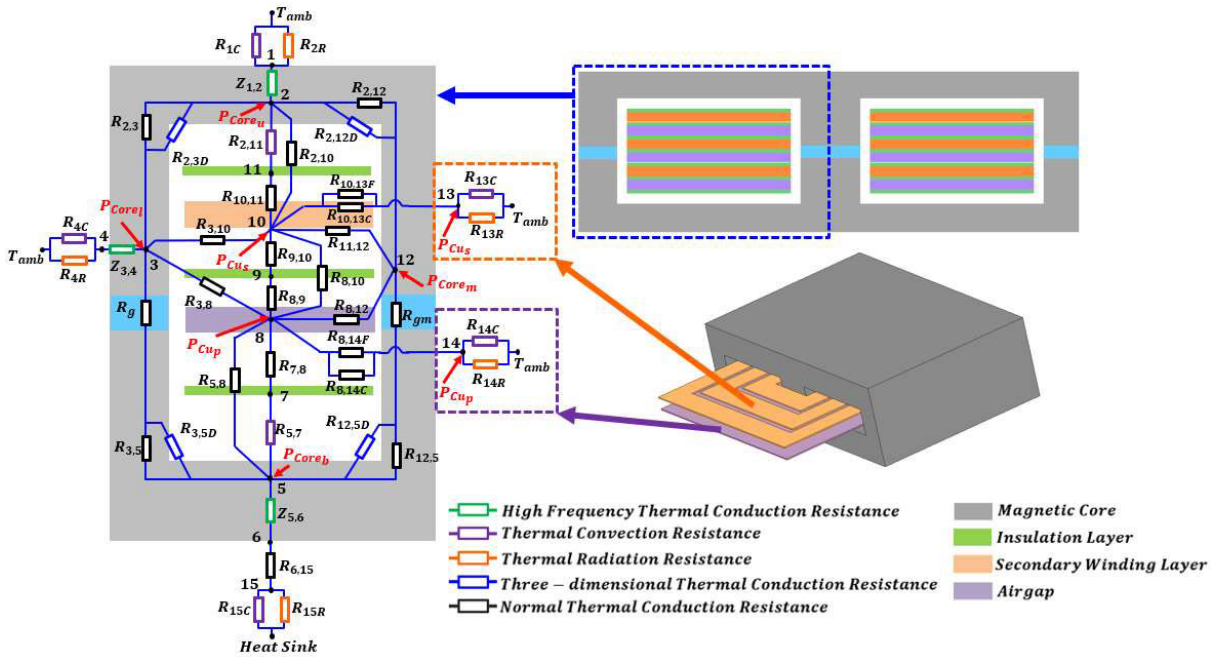
FIGURE 13. Frequency dependent thermal network as proposed by Shafei et al. in [40].

this model, a 3D finite element electrothermally coupled model was simulated using Flux software [41]. The convection and radiation effects were included in the numerical model. In addition, experiments were conducted using an infrared thermal camera. The results showed a good agreement between the frequency-dependent TN model, finite elements, and measurements. The two main advantages of this model are that it considers the 3D shape of the PMC and requires fewer nodes.

Another 3D TN was introduced in [42]. The TATPM model for a thermally automated tool for planar magnetics is automatically generated from a matrix description of the geometrical parameters of the windings and planar core (Fig.14). The model considers the 3D aspects of geometry. Three heat-transfer modes (conduction, convection, and radiation) were considered. Additionally, the model can be solved for transient and steady-state analyses. In this study, the model was applied to two planar transformers (360 VA E/PLT38 core-based and 2 kVA E/PLT58 core-based), and the results were compared with FEA and temperature measurements of the prototypes. One of the main advantages of this model, in addition to automation, the possibility of transient analysis, and short computation time, is the set number of elements that can allow a detailed thermal distribution. TATPM represents a good trade-off between the FEA and conventional thermal networks.

A planar inductor designed for high current and ripple was studied in [43]. Advanced thermal management was deployed by combining many actions: an aluminum liquid cooling cold plate and an aluminum bracket completely covering the inductor. In addition, a thermally conductive ceramic shim was used to ensure good thermal contact between the
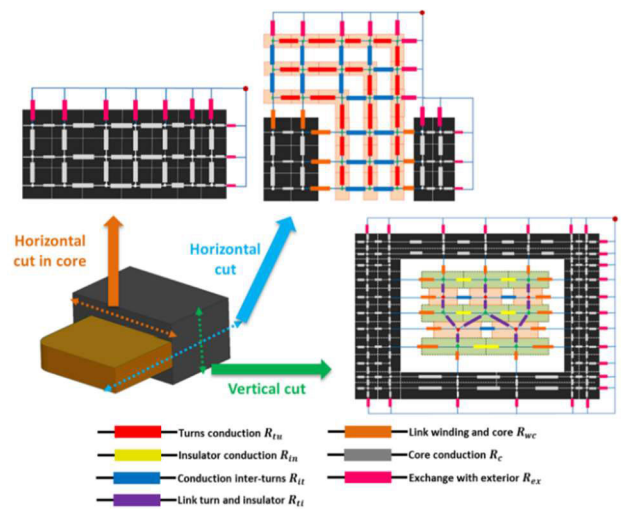

FIGURE 14. Thermal automated tool for planar magnetics [42].

windings and baseplate. Finally, thermal vias were added to the center and sides of the winding PCB. A thermal model of the planar inductor and various thermal management components was implemented based on a 2D thermal network.

The TN results showed good agreement with the FEA applied to the complete component and one eight (1/8). TN was then used to study the effect of each thermal management action. The results indicate that the thermally conductive ceramic shim significantly contributed to the temperature reduction. A detailed study of advanced thermal management, in addition to the 2D TN model allowing its modeling, is beneficial for achieving high-power density planar inductors.

4) COMPARISON BETWEEN 1D AND 3D THERMAL NETWORKS

To compare the effectiveness of the thermal resistance networks, the unidimensional TN illustrated in Fig.10 and the 3D TN introduced in [42] are compared in a planar transformer case study. The latter is based on the E/PLT 58 core combination. The thicknesse of the primary and secondary conductors' thickness is 0.2 mm and their widths were 4 mm and 17 mm, respectively. The total loss dissipated in the transformer is 10 W, with copper losses of 7 W and core losses of 3 W. To perform the thermal analysis, a heat exchange coefficient of 10 W.m^{-1}.K^{-1} was applied to its external area at an ambient temperature of 30°C. Fig.15a shows the 3D geometry of a quarter of the studied transformer, and Fig.15b presents the winding configuration inside the core window.

More details regarding the mathematical formulation can be found in Appendix A for the 1D TN and Appendix B for the 3D TN.
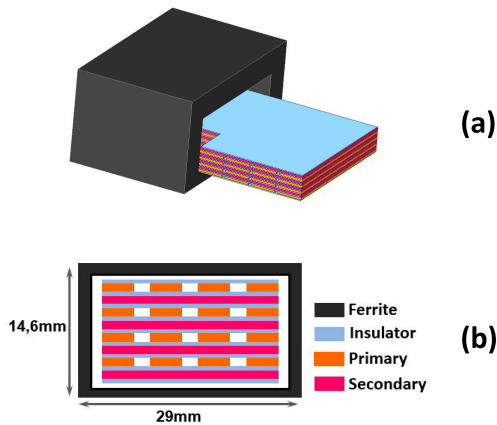

FIGURE 15. Planar transformer case study: (a) 3D CAD geometry, (b): core window and winding details.
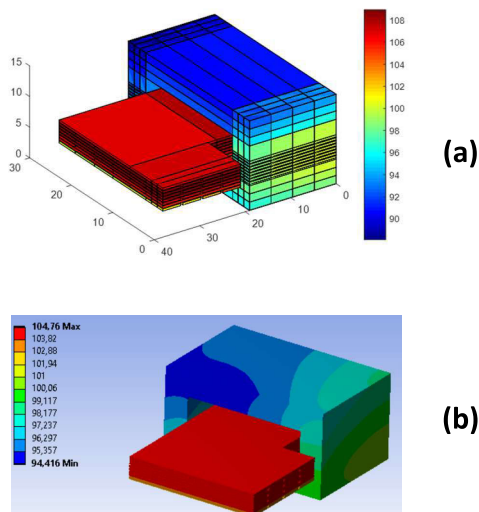

FIGURE 16. Temperature distribution: (a) 3D thermal resistance (TATPM), (b): FEA result.

TABLE 3. 1DTN, 3DTN and FEA maximal temperature result.

	1D TN	3D TN	FEA
Maximal temperatures in °C	124,56	108,12	104,76
Error °C	19,8	3,36	-

Table 3 lists the maximal temperatures computed by the 1D and 3D TN, in addition to the FEA results. The 1D model strongly overestimated the temperature values by approximately 20 °C compared to the FEA. This difference is due to the geometry of the 3D component, which is neglected and, consequently, important heat paths and cooling areas. The 3D thermal network was more accurate. It reproduces a similar temperature distribution as FEA, as shown in Fig.16a and Fig.16b.

Moreover, the resulting temperature presents less than 4 °C error regarding FEA results.

Even if 3D TN are more accurate, their development and implementation are not always simple. Compact thermal models, even if behavioral, can be an interesting alternative when a good tradeoff between time and accuracy is required.

5) COMPACT THERMAL NETWORKS

Compact thermal models (CTMs) are a particular case of behavioral thermal networks with a reduced number of lumped elements. The most popular methodologies for deriving the CTM are the DEvelopment of Libraries of PHysical models for an integrated design environment (DELPHI) and Supplier Evaluation and Exploitation of DELPHI (SEED) [44], [45]. CTMs were first applied to power semiconductors before they were extended to other power electronic components. This section focuses on the application of CTMs in PMCs.

In [46] a CTM was built for two PCB winding planar transformers based on E18 and E22. The model contains three thermal resistances: one for the magnetic core, one for the windings, and one for modeling the thermal link between the core and the windings as illustrated in Fig.17.
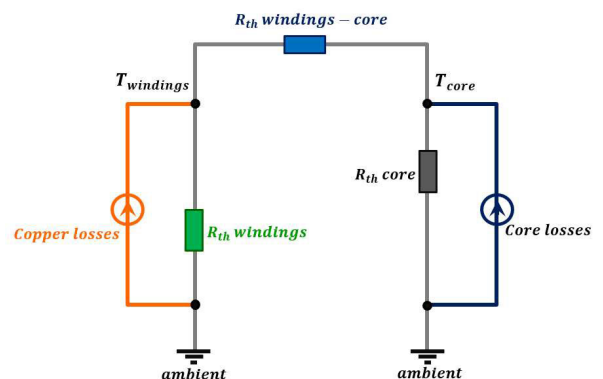

FIGURE 17. Compact thermal model of planar transformer as proposed in [46].

The thermal resistance was determined from the measurements. Core resistance was calculated from a test on a planar core with a single turn supplied by a pulsating voltage. The winding thermal resistance was deduced from a test in which the windings were excited using DC current. Finally, the link resistance was extracted from the temperature drop when the core was added to the windings, which were always under direct current (DC) excitation. This thermal model cannot be qualified as one-dimensional; however, it is a behavioral model that can estimate the temperature of the transformer parts.

This model was implemented using a SPICE simulator [32] and showed good agreement with the measured temperatures for several loss values. This model can help study the component thermal behavior for various operating points using circuit simulation software owing to its reduced node number. However, they cannot be used in the design process because they require experimental data for element identification.

One of the merits of this study is the investigation of the thermal management of PMCs by testing solutions to reduce the temperature of the components. For example, thermal grease was added between the core and FR4 substrate. An aluminum cover was then added to the top of the core and attached using a thermal pad or thermal glue. In the final solution, the core was surrounded by thermal glue. The results showed that the addition of an aluminum cover significantly reduced the temperature of the planar transformers. This solution is widely used in commercial PMCs [47], [48], [49].

In [50], the authors introduced a CTM inspired by the DELPHI method to obtain a BC-independent thermal model. In this model, three nodes are defined to represent the three

windings. They are also used to inject copper losses. Another node is located inside the core to inject the core losses. In addition, eight nodes were placed on the external surfaces, four on the winding external surfaces and four on the core surfaces. Finally, the last node was used to model the ambient environment. All these nodes were linked by 78 thermal resistances. The latter were identified using intensive numerical simulations combined with a multi-objective genetic optimization algorithm. The simulations were performed with 13 boundary conditions selected from the set prescribed by the Joint Electron Device Engineering Council (JEDEC) standard [52] relative to the DELPHI compact model [53]. Simulations were performed for three loss configurations. In the first configuration, only the winding losses were considered. Second, only the core losses were applied. In the final configuration, both types of loss were injected. Consequently, 13×3 numerical simulations were carried out on a high-performance system with two Intel Xeon E5-2680 running at 2.7 GHz, with 24 cores and 256 GB RAM. The optimization objective was to minimize the criterion representing the temperature and heat flux errors between the proposed CTM and numerical simulations. Further details regarding the global methodology used to extract the DELPHI-like model can be found in [54] and [55]. This model has the advantage of reducing the number of required nodes. It is very fast and simple to implement in circuit simulation software. It can be used to study the thermal behavior of PMC and some cooling solutions. However, a large number of intensive numerical simulations combined with optimization-based fitting are required for its development.

A transient CTM was proposed by Górecki et al. [51] for a 2-winding planar transformer. The model takes into account the self-heating in every element of the transformer (windings and core), and the thermal coupling between them, which leads to three subcircuits for every part as illustrated in Fig.18 for the primary winding. Every subcircuit contains many parallel resistance and capacitance cells to form a Foster network [56]. The first and the second subcircuits (Fig.18a and Fig.18b) allow to compute the excess of temperature of the primary winding due to the power losses in the core and in the secondary winding respectively. The third subcircuit (Fig.18c) evaluate the temperature rise due to self-heating and the coupling with the core and the secondary winding represented by a controlled voltage source. The network elements were identified from the experimental measurements. The results showed a significant dependence of the thermal impedances on the operating frequency. This effect was studied by the same authors [57]. The experimental results revealed that the temperature difference between transformer parts can exceed 70 °C. However, this result is not always true for the free convection. This can be explained by the weak contact between the component elements and low window filling in the transformer used by the authors during the experiments.

This model was also used in [58] to study a 1 MHz PCB planar transformer. Improved versions of this CTM were
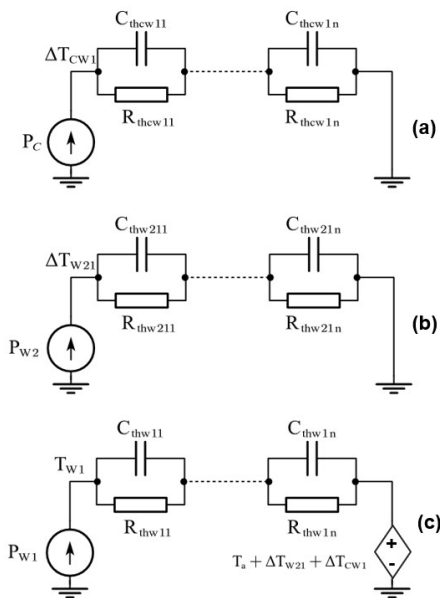

FIGURE 18. Compact thermal model of planar transformer described in [51]: primary winding temperature excess due to: (a) the core, (b) secondary winding, (c) : self heating and coupling.
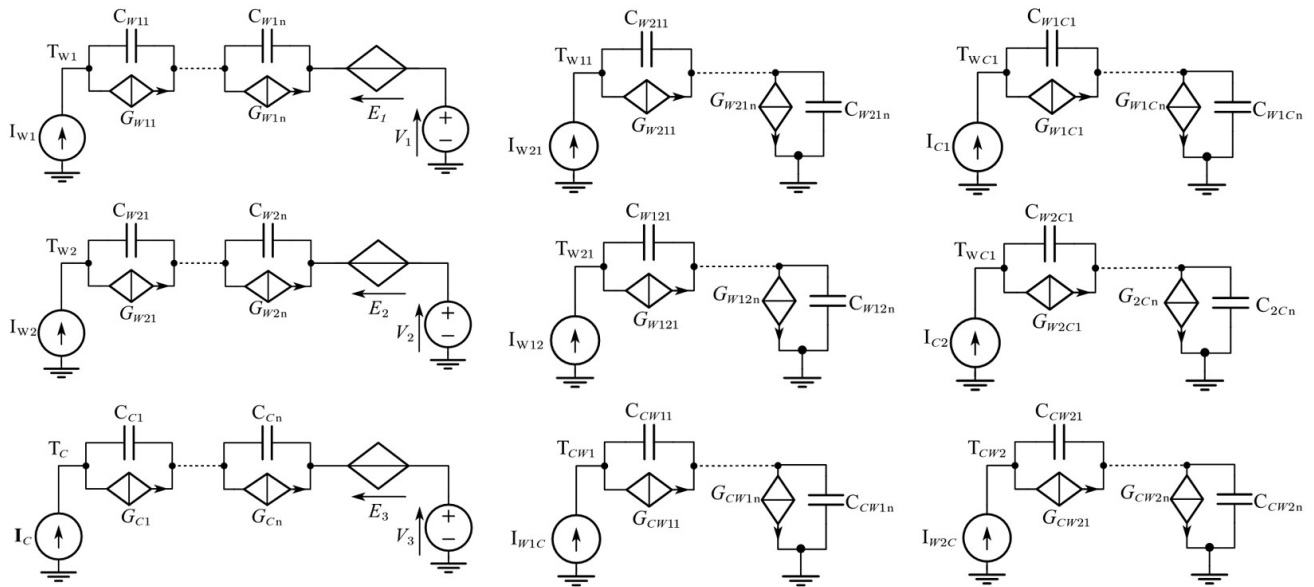
FIGURE 19. Nonlinear compact thermal model of planar transformer as proposed in [59] and [60].
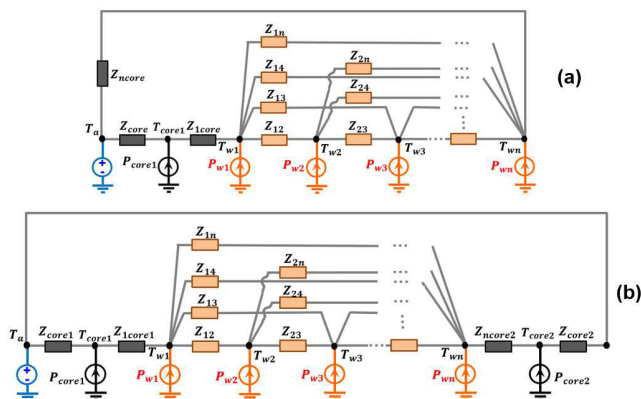

FIGURE 20. Compact thermal model of planar transformer as described in [62] : (a) one node on the core, (b) two nodes on the core.

proposed in [59] and [60] as presented in Fig.19. In these studies, non-linearities were introduced into the CTM. As in [51], every part of the transformer (primary and secondary windings and the core) is represented by 3 foster networks, to take into account the self-heating and the thermal coupling with the other parts of the transformer, which leads to 9 subcircuits. The nonlinearities are considered by the variation of thermal resistances with temperature under the form of controlled current sources. The model elements were identified from experimental measurements at various power dissipation levels using the methodology presented in [61].

Another CTM was applied to a multiple-winding planar transformer [62]. To build the model, one node is placed in each winding with a current source representing the copper losses as shown in Fig.20. Two configurations were proposed: the first with only one node in the core (Fig.20a) and the second with two nodes in the core (Fig.20b). All the nodes were coupled by several thermal impedances to

account for the dynamic aspects of the problem. The thermal impedances were then extracted from transient computational fluid dynamics (CFD) analysis. Good agreement between the model results and experimental data was obtained. Even if this CTM is simple and has a reduced node number, it cannot be easily used for planar magnetic design, because it requires intensive CFD calculations. However, it is of great interest to study dynamic applications because of their transient capabilities.

In a recent study [63], Shen et al. introduced two TN-based models by simplifying a detailed thermal network. Two geometrical simplifications were used. The first considers only the core (Fig.21a), whereas the second considers an equivalent cuboid block with core external dimensions (Fig.21b). For the two models, the total losses (copper and core losses) are dissipated in the simplified geometry. The radiation and convection effects were computed analytically, and their dependency on the temperature was considered. The simplified geometries were analyzed using CFD simulations to validate the analytical computations of the two models. Finally, the latter were compared to measurements on a MHz planar transformer and demonstrated good accuracy.

The proposed models are straightforward and can easily be used in an iterative design process. Even if the simplifications are strong, they are reasonable when the transformer has a high winding filling factor and good thermal contact between the core and windings.

Thermal networks have many advantages in the thermal modeling of PMCs. They are very comprehensive for electrical researchers and engineers and can be easily used in circuit simulation software. Although a TN can be complex and can reproduce the 3D aspect of a PMC, it cannot usually provide a detailed temperature distribution or reproduce complex 3D shapes. Additionally, the definition of lumped elements is
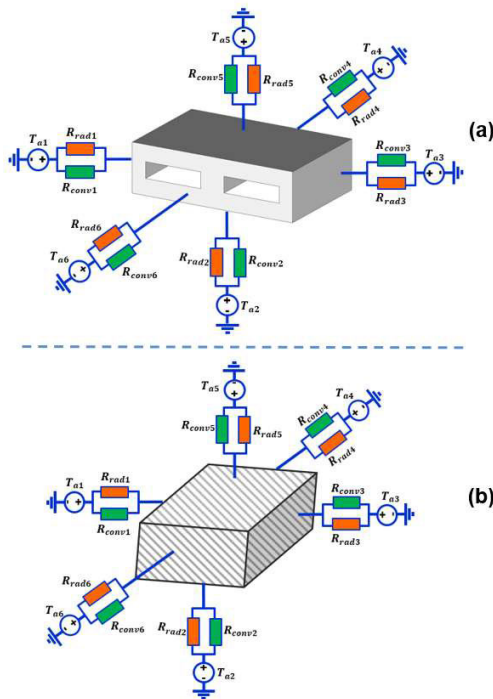
FIGURE 21. Simplified equivalent CTM of planar transformer as introduced in [63]: (a) core based model (b) equivalent cuboid based model.

not always simple. Semi-analytical and numerical models are more suitable to overcome these limitations.

C. SEMI-ANALYTICAL AND NUMERICAL MODELS
1) SEMI-ANALYTICAL MODELS
Although semi-analytical models are relatively common for the electromagnetic modeling of PMCs, they are not widely used for the thermal aspect. In [64], Buccella et al. established a semi-analytical model based on Green's functions and a variable separation method to solve heat equations. In [65], the same authors performed a 2D FEA using the ANSYS Maxwell software [66] to deduce a 1D spatial and time-dependent current density. Two types of boundary conditions were prescribed to compute the temperature distribution: a fixed temperature on the bottom surface of the core, and a constant heat transfer coefficient of 50 $Wm^{-2}K^{-1}$ (forced convection) at the top. The ambient temperature was maintained at 25 $^{\circ}$C. The model results were consistent with the measurements, although the deviation of the model increased with time. However, this deviation was not clearly explained in the present study. One explanation is the use of a constant heat-exchange coefficient. The component temperature increased with time, thereby increasing the amount of heat exchanged by radiation and convection. Consequently, the heat exchange coefficient should increase with temperature, and thus, with time. The use of a constant coefficient leads the model to overestimate temperature. Although unidimensional, a semi-analytical model requires good mathematical background. Compared to the other 1D models presented
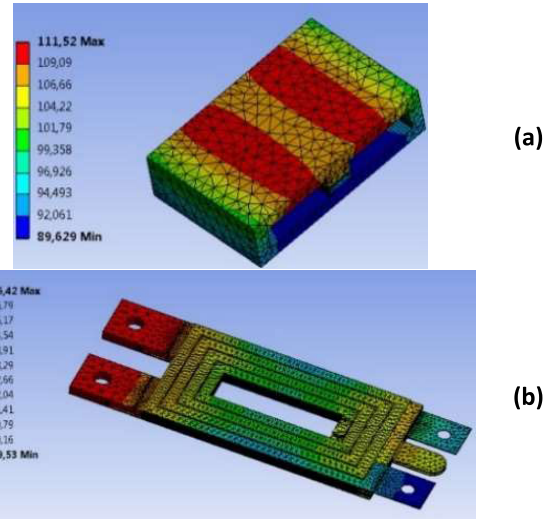

FIGURE 22. Example of 3D FEA resulting PMC temperature distribution: (a) core and (b) PCB windings.

in [25], [26], [27], [28], [29], and [30]; the latter has the advantage of providing continuous spatial and temporal temperature distributions. It also considers the distribution of losses inside the component. Such a model can be used for design purposes or to study the thermal behavior of components under various operating conditions. However, its limitations are linked to the 1D hypothesis, restricting its applicability. For thermal management studies and component optimization, 2D and 3D aspects must be considered.

2) FINITE ELEMENT MODELING
The finite element method (FEM) is widely used in electrical engineering for thermal modeling to perform FEA. In this study, FEM refers to the numerical resolution of the heat equations in the solid regions. In addition to this conduction phenomenon, convection and radiation were approximated using the heat transfer coefficient in the external area of the studied component as boundary conditions. As shown in Fig.22, complex PMC 3D geometries can be modeled using the FEM. This method enables the computation of a detailed temperature distributions. Many authors have used the FEM to study the thermal performance of planar magnetics [65], [66], [67], [68], [69], [70], [71], [72], [73], [74], [75], [76], [77], [78], [79], [80].

For example, in [67], thermal finite element simulations were performed to compute the temperature distribution of a 65 W, 300 kHz planar transformer in free convection cooling mode. The heat transfer coefficients were computed from the experimental correlations and applied only to the top and bottom surfaces of the windings. Simulations were performed using the ANSYS software [66] in the steady state. Unfortunately, no details regarding the computed temperature values are provided. The authors estimated that the simulations would be calibrated based on the experimental results.

An automotive planar inductor was studied in [68]. The particularity of this work lies in the high ambient temperature

associated with harsh automotive environments. To achieve the thermal requirements, unconventional conduction thermal management is considered by encasing the entire inductor in an aluminum sleeve. Three air gaps and two cooling configurations are investigated. The first cooling method is based on an extended core that covers the winding ends, whereas in the second method, the windings are in direct contact with an aluminum sleeve.

From the loss analysis, only one distributed air-gap configuration was studied (the lowest losses) using thermal modeling. The 3D FEA was performed by considering only a quarter of the planar component and an ideal heat sink at its bottom face. The heat-sink temperature was set to 85 °C. The maximum temperatures obtained from the simulation were similar for the two cooling configurations. However, a configuration with an extended core has a large hotspot region. This difference could not be detected without a 3D analysis. Finally, the FEA results were confirmed by measurements using two prototypes.

Buccella et al. developed a 1D finite element model to study two 6 kVA 40 kHz planar transformers [65]. Both transformers used three hybrid windings, mixing PCBs and copper foils; however, one was based on an E-shaped core, and the other on a U-shaped core. Copper losses were computed by 2D FEA using ANSYS Maxwell software [66]. Losses were estimated for the current fundamental and second harmonics. Core losses were calculated using the Steinmetz equation during post-processing. The proposed thermal model is a steady-state one-dimensional (1D) finite-element model. The geometry of the 29 rectangular layers was considered to have a perfect contact between them. Two types of BC were applied: a fixed temperature on the bottom surface of the core and a constant heat transfer coefficient of 20 W m^{-2} K^{-1}, accounting for convection and radiation on the top surface. The ambient temperature was maintained at 25°C. The developed numerical model was used to investigate the current fundamental and second-harmonic contributions to temperature rise. To validate FEA, measurements were performed only for the E-core configuration. The temperature was measured at multiple points using a digital temperature sensor embedded between the winding layers. The calculated temperatures were in good agreement with the measured values. The authors clearly presented the developed model, but the test and boundary conditions were not explained. Additionally, the core temperature was not measured for comparison with the FEA results.

A 1.5 kW planar transformer was studied using FEM [69]. To reduce the complexity of 3D modeling, two simplifications were introduced. First, only a quarter of the transformer was considered. Second, the copper tracks were modeled as two-dimensional (2D) layers. The copper losses were calculated from the measured DC resistances, considering that the AC resistance was close to the DC resistance owing to the low switching frequency (20 kHz). The core losses were measured directly. The heat exchange coefficient was used as a fitting parameter to obtain a similar temperature distribution

between the thermal imaging measurements and the FEA results. A numerical model was used to explore the current and frequency limits to maintain the transformer at a maximum temperature of 100 °C for safe and reliable operation. Solutions to improve thermal management have also been studied using cold plates and heat extractors for windings. This model has the advantage of being 3D. Moreover, the introduced 2D layer simplification is advantageous for reducing problem size and calculation time. This hypothesis is suitable for PCBs with a low copper track thickness. Finally, such a model is very convenient for studying thermal management. The variation in the heat-exchange coefficient with the component and ambient temperature should be considered to improve the model.

Wrobel et al. studied a planar inductor with a laminated core and copper-foil winding [70]. The temperatures of the components were evaluated using a 3D FEA. The geometry is simplified to reduce the complexity of the problem. This component is subdivided into five lumped regions. The winding and laminated cores are separated into two parts with different anisotropic thermal conductivities. The other regions are the encapsulating epoxy, slot liner, and aluminum container. The inductor was cooled using a water-cold plate at 70 °C, attached to the bottom of the aluminum container. The remaining surfaces were then cooled using natural convection. For FEA, the heat transfer coefficients were evaluated experimentally, and the loss model was scaled with temperature to accurately predict the thermal behavior of the inductor. Comparisons with measurements demonstrated the accuracy of the numerical model and the importance of considering the loss variation with temperature to perform reliable thermal modeling.

Tria et al. [71] performed 3D thermal FEA for an E32-based planar transformer made with 35μm copper thickness PCB windings. The losses were computed using 3D FEA, and a heat-transfer coefficient of 10 Wm^{-2}K^{-1} was specified. The FEA results were compared with the IPC-2152 standard [72] used to calculate the current capability of PCB tracks for a given temperature rise. Hence, the temperature increase was computed for several current values and compared with the IPC standard. The authors highlighted a large deviation between the IPC-2152 standard and FEA simulation results, even though these standards are usually used in the PMC design guidelines. Otherwise, good agreement is obtained with the temperature rise computed from the thermal resistance of the manufacturer. This result can be explained by the fact that the IPC-2152 standard addresses single-layer PCB design. The results presented in this paper are interesting, but they remain only qualitative and require experimental validation. Indeed, the heat exchange coefficient value is unjustified and its choice may be questionable.

The thermal behavior of a MHz-range planar transformer was investigated in [73]. In this study, a 3D thermal FEA was performed at three frequencies:1 MHz, 1.3 MHz, and 1.5 MHz. As in [74], losses were computed using 2D FEA [66]. Notably, the thermal analysis considered only the

secondary winding losses because they had the highest losses in the component. Consequently, the results show a non-uniform temperature distribution. The maximum temperature is located at the end of the secondary winding. This could be explained by the absence of primary and core losses, in addition to core participation in the cooling of the winding parts located inside the window.

FEM was used in [75] to predict the temperature distribution of two 700 kHz planar transformers. The first transformer is based on a combination of an E32 and a PLT core [17], whereas the second transformer is made of an ER32 planar core. The windings were conceived in a multilayer PCB to handle a current of 20 A. For the FEA, the simulation conditions (i.e., heat exchange coefficient and ambient temperature) were not specified. Moreover, as in [73], the primary and core losses are neglected. Therefore, it has been shown that the end winding could be the hottest part of a PMC.

In [76], the authors dealt with reducing planar transformer leakage inductance by changing the turn current density distribution. This leads to an increase in copper losses, which limits the benefit of reducing leakage inductance. Therefore, 2D axially symmetric thermal FEA was performed to compute the temperature distribution of the planar transformer. Owing to the high level of losses, this study assumed a forced-air cooling setting with a surface heat coefficient of $30 W.m^{-2}.K^{-1}$. This model was used to investigate the effect of the surrounding PCB winding using a thermally conductive material. The results indicate the presence of a hotspot in the winding. An adhesive material of 1.5 W m^{-2} K^{-1} is necessary to reduce the temperature rise within an acceptable range. This study is only qualitative, but it can provide an idea of the location of hot spots and some recommendations to reduce temperatures in critical regions. These conclusions will be beneficial for the design of reliable PMC.

A comparison between a planar EE38 core-based planar transformer and a conventional PQ35/35 core-based transformer was presented in [77]. 3D FEA was performed using the Flux software [41]. The bottom temperature of the transformers was fixed at $40^o C$ in contact with the heat sink. Subsequently, two scenarios are simulated. In the first, only core losses are considered, whereas in the second, copper losses are added to a homogenous winding material. The results indicated that the planar transformer temperature was significantly lower than that of a conventional transformer. In addition, planar transformers have a lower thermal time constant owing to their smaller volume.

A 3D FEA was employed in [78] to investigate the thermal management of a planar transformer in a spacecraft environment. The authors took advantage of 3D numerical modeling to compare the thermal behavior of two planar transformers based on EQ and ER cores. Three cooling strategies were investigated: window filling to increase the thermal contact between the core and winding, gap filler pad to link the winding to a metallic baseplate, and metallic connectors between the windings and baseplate. The authors showed that the impact of thermal management on the temperature rise

is significant in such an environment. The gap filler linking the winding and the baseplate appears to be the best cooling strategy. This study is interesting and demonstrates the great value of thermal conduction cooling for space applications where convection and radiation transfer are not significant.

In [79], a planar transformer with a high turn ratio was studied. First, 3D FEA was performed to investigate the effects of thermal vias. The effect of adding copper bricks to the outer layers is also simulated. The main cooling was enhanced using a water-cooled cold plate attached to an aluminum heatsink. A thermal interface material was introduced between the transformer and heatsink, and between the heatsink and cold plate. The analysis indicates that the addition of copper bricks decreased the component temperature and made it more uniform. These results were confirmed by the infrared thermal imaging of the prototypes.

A set of ten planar magnetics designed for a 125 kW automotive boost converter was studied in [80]. This study focuses on the packaging and thermal management of magnetic components. The primary cooling process was performed using a cold-cooled liquid plate. Five different thermal-management configurations were studied using FEA. In the first three configurations, several electrothermal and thermal processes via disposition were investigated. An Aluminum cover was added to the fourth configuration. Finally, an Alumina layer was inserted between the transformers and the cooling cold plate. The FEA results showed that the aluminum cap drastically decreased the core temperature, whereas the addition of an alumina layer significantly decreased the winding temperature. These conclusions were confirmed by measurements.

One of the merits of this study is the in-depth analysis of thermal paths for heat extraction. This study is illustrated in Fig.23 for a planar transformer attached to the cold plate. As shown in Fig.23a, the main path passes through the core, which is clamped directly to the cooling system. The heat removing from the winding was improved by the thermal vias and thermal pad. These two additions reduce the thermal resistance between the winding and core on one hand, and between the cold plate and PCB windingin the other hand. At the top of the transformer, heat is extracted via thermal convection and radiation. An aluminum cap was added to improve the heat removed from the top, as shown in Fig.23b. In this case, the heat removed from the top of the core can also be evacuated by the cold plate, allowing for more effective cooling.

A similar thermal path analysis was performed in [81] to design an innovative high-current planar inductor with 3D printed windings.

Thermal models based on FEM are typically employed to directly compute the temperature distribution of the PMCs. They can also be used to identify elements and calibrate compact thermal models [50], [51], [52], [53], [54], [55]. FEM is increasingly being used for the thermal modeling of PMCs. Indeed, it allows the computation of complex 3D accurate temperature distributions inside components. Moreover, the FEM is adequate for studying thermal management
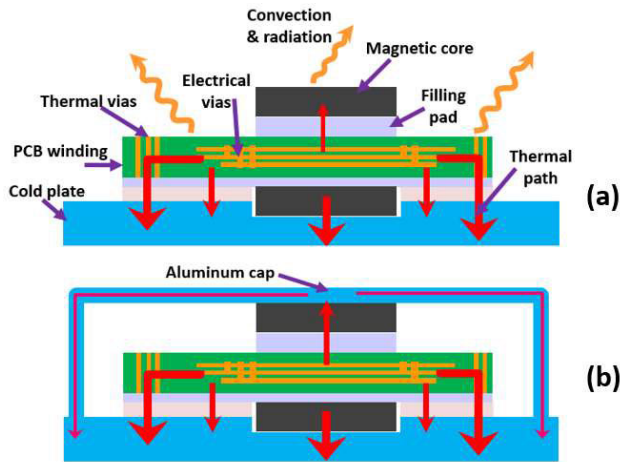
FIGURE 23. Thermal paths of extracted heat: (a) without aluminum cap, (b) with aluminum cap as described in [80].
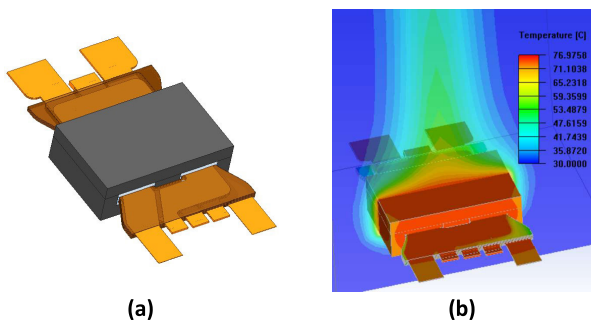

FIGURE 24. Example of CFD applied to CMP: (a) 3D geometry, (b) 3D CFD temperature in free.

configurations. Nevertheless, their results depend on the heat transfer coefficient used because the FEM cannot represent the interaction with fluids directly. This topic is of major importance, particularly for forced-convection cooling. This issue can be addressed using Computational Fluid Dynamics (CFD).

3) COMPUTATIONAL FLUID DYNAMICS (CFD)

In contrast to the FEM, CFD does not approximate convection using heat transfer coefficients. It can model fluid flow and heat transfer in the solid and fluid domains. In CFD, a set of nonlinear and coupled equations is numerically solved. These equations link the pressure, velocity, and temperature [14]. CFD is a powerful tool for accurately modeling convection and fluid flow for complex geometrical shapes in natural or forced configurations. It can also be an excellent alternative to experimental measurements for calibrating thermal resistance [24], thermal networks [50], [51], [52], [53], [54], [55], [56], [57], and FEA boundary conditions [55]. Even if CFD is known to be difficult to use because of the computing resources needed and the solved problem non-linearities, it is increasingly used for PMCs modeling [82], [83], [84], [85], [86], [87]. An example of CFD applied to CMP is shown in Fig.24. Indeed, Fig.24a

shows an HF planar transformer 3D geometry and Fig.24b presents the 3D temperature distribution computed using CFD under natural convection.

In [82], the authors worked on a PMC design process based on simple TN. They estimated that the identification of various thermal resistances was a difficult task. Therefore, They preferred to use computational fluid dynamics (CFD) thermal modeling to accurately predict the temperature of their components. In this process, losses were computed using 3D FEA. The values were then transferred to the CFD simulation. The planar transformer was modeled in a large air box to accurately model the convection heat transfer. However, other details of the thermal simulation are not specified. The simulation results showed a hotspot on the dielectric material. The authors have suggested reducing the dielectric thickness, placing the transformer in oil, or forced-air convection cooling to decrease the temperature rise.

Ganga et al. worked on an HF 20 kW SiC converter [83]. To achieve the efficiency requirements, ten planar transformers were integrated into the converter. The inputs are connected in parallel, whereas the outputs are connected in series (a configuration called IPOS). A heat sink with integrated pipes for liquid cooling is used to limit the maximum temperature of the transformers. CFD) simulations were performed to determine the liquid cooler velocity to guarantee the most uniform temperature distribution without exceeding 50 °C. The relevance of this work lies in the study of a pack of planar transformers and the strong thermal constraints imposed by their specifications.

Two configurations of 6.6 kW 500 kHz planar transformer configurations were introduced in [84]. The goal was to form a resonant tank for the CLLC power converter with global optimization of the converter, including the transformer. CFD was first used to compare the PCB inner and outer trace temperatures under the same power losses and forced air cooling. Consequently, only 2-layer PCBs are used in the transformer. CFD simulations were performed for the final design under forced cooling conditions with an airflow of 91 CFM. In this study, CFD was very useful because of the complex geometry of the transformer and the forced air cooling.

3D electrothermal modeling was performed in [85] to study a 5-winding planar transformer dedicated to a multichannel power supply. FEM has been used for magnetic modeling and loss computation. The FEM was coupled with a CFD solver to perform thermal modeling using the ANSYS software [66]. A detailed analysis was necessary to verify the thermal integrity of the transformer. Even though a prototype was presented in this study, the CFD thermal analysis results were not compared with the measurements.

In [86], CFD was applied to study the cooling of two parallel 500 kHz planar transformers designed for an 18 kW high-power density converter. The two transformers were double-sided cooled by using two copper heat sinks attached to their top and bottom faces. In addition to the heat sinks, air was blown by a fan to maximize heat extraction. An air duct is also added to improve the thermal behavior of the

transformer. The effectiveness of the air duct was proven by CFD simulations and measurements.

In a recent study [87], CFD was employed to study the direct liquid cooling of a planar transformer placed in a dedicated additive-manufactured housing. CFD was used to compute the maximum temperature and pressure drop for different liquid flow rates. Two liquids were compared, Novec 7300 and ethylene glycol. According to the results, Novec 7300 is the best choice. The study showed that liquid cooling is more effective than a classical cold plate and results in a lower pressure drop. This also leads to a lower cooling power consumption. These results were confirmed by experimental measurements. This study is the first to address the direct cooling of planar HF magnetics. This opens up the perspective of efficient high-density power converters.

D. SYNTHESIS OF THE LITERATURE REVIEW

After presenting various studies on the thermal modeling of PMCs, a global analysis was performed. For this purpose, different models were compared based on the following criteria.

- **Model type:** PMC thermal models are classified into five main categories: thermal resistance, thermal equivalent networks, semi-analytical methods, finite element methods, and computational fluid dynamics.
- **Dimensions:** The models can be 1D, 2D, or 3D, depending on the modeling objective and geometrical complexity. Some models are also behavioral. This means that it refers to the components' parts but does not reproduce its physical geometry.
- **Temporal aspect:** These models can be used for steady-state or transient (dynamic) analysis.
- **Heat transfer modes:** These models can consider all heat transfer modes, including conduction, convection, and radiation, or only some of them.
- **Loss distribution:** The losses in the windings and core did not have a uniform distribution in the component volume. Some models use distributed (nonhomogeneous) losses, whereas others use a uniform distribution to simplify the thermal modeling problem.
- **Type of coupling:** The coupling can be weak or strong. Weak coupling does not consider the variation in the electrical and thermal properties with temperature, unlike strong coupling.

The models were analyzed according to six criteria. The synthetic process is presented in Table 4. Thermal models and related papers were ordered according to their categories and chronological order. It must be noted that some papers could appear in more than one category when different types of models are used for an application. This is the case, for example, when FEM or CFD is applied to validate or calibrate thermal networks.

E. ANALYSIS AND DISCUSSION

Fig.25 shows the temporal distribution of the reviewed papers according to the model type. It can be seen that PMC thermal
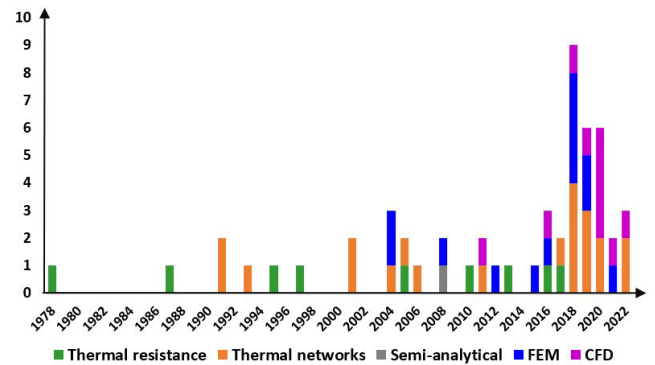

FIGURE 25. Temporal distribution of the reviewed papers.

modeling is increasingly addressed in the literature. This can be explained by the increase in the use of PMC in power converters, owing to the increase in power densities and thermal constraints.

Concerning the type of model, as shown in Table 4, the thermal resistance concept is widely used to estimate the PMC temperature. Thermal resistances are suitable in the early design stage, owing to their simplicity. Other models must be used to perform a deeper analysis, providing the temperature difference between the component parts, which can induce high-temperature gradients and hotspots. This is the case for the thermal networks. TNs are commonly used for PMC modeling because they enable us to obtain more details than thermal resistance. Moreover, such a model is comprehensive for electrical engineers, making its application practical.

Numerical models have been increasingly developed since the 2000s with the democratization of powerful computers in addition to parallel computation capabilities. The finite element method is extensively used to compute the temperature distribution in 3D. The use of FEM is supported by the vast offer and strong development of free and commercial software. Similarly, CFD has been increasingly used in recent years. CFD is applied for the direct modeling of PMCs or as a calibration tool for other models such as thermal resistance or TN. However, its utilization remains limited owing to the time required to perform simulations and convergence problems.

Semi-analytical models are scarce because of the complex transformer geometry, which results in complex mathematical problems.

Regarding the heat transfer modes, conduction and convection are almost always considered in the modeling, whereas radiation is sometimes neglected. This hypothesis can only be justified in the case of forced convection. In free air, radiation can participate in cooling to the same extent as in convection. This topic will be discussed in the next section.

In general, for the thermal modeling of PCM, the temperature is computed only in the steady state. This is linked to the simplicity of modeling. Moreover, the increase in temperature is usually calculated in the steady state under losses and ambient temperature under the worst operating conditions. Nevertheless, a transient analysis could be interesting for

TABLE 4. Literature paper classification.

Type	Reference	Year	dimensions			Modes			Transient		Distributed losses		Coupling	
			1D	2D	3D	Cond	Conv	Rad	Yes	No	Yes	No	Weak	Strong
Thermal Resistance	[22]	1978	Behavioral											
	[19]	1987	Behavioral											
	[20]	1995	Behavioral											
	[16]	1997	Behavioral											
	[21]	2005	Behavioral											
	[17]	2010	Behavioral											
	[18]	2013	Behavioral											
	[24]	2016	Behavioral											
	[23]	2017	Behavioral											
Thermal Networks	[25]	1991	■			■				■		■	■	
	[27]	1991	■			■				■		■	■	
	[28]	1993	■			■	■	■		■		■	■	
	[46]	2001	Behavioral			■	■	■		■		■	■	
	[36]	2001			■	■	■	■		■		■	■	
	[29]	2004	Behavioral			■	■			■		■	■	
	[26]	2005		■		■	■			■		■	■	
	[31]	2006		■		■				■		■	■	
	[39]	2011		■		■	■	■		■		■	■	
	[55]	2018	Behavioral			■	■	■	■			■	■	
	[59]	2017	Behavioral			■	■	■	■			■		■
	[50],[53]	2018	Behavioral			■	■	■		■		■		■
	[55]	2019	Behavioral			■	■	■		■		■		■
	[60]	2020	Behavioral			■	■	■	■			■		■
	[40]	2018			■	■	■	■	■			■	■	
	[37]	2018			■	■	■	■		■		■	■	
	[58]	2019	Behavioral			■	■	■		■		■	■	
	[42]	2019			■	■	■	■	■			■		■
	[30]	2020	■			■	■			■		■		■
	[63]	2022	Behavioral			■	■	■		■		■		■
	[43]	2022		■		■	■	■		■		■		■
Semi-analytical	[64]	2008	■			■	■	■	■		■		■	
FEM	[67]	2004				■	■			■		■	■	
	[68]	2004			■	■	■			■		■	■	
	[65]	2008	■			■	■	■		■		■	■	
	[70]	2012			■	■	■	■		■		■		■
	[71]	2015			■	■	■			■	■		■	
	[73],[74],[75]	2016			■					■		■	■	
	[50],[53],[54]	2018			■	■	■	■		■		■	■	■
	[37]	2018			■	■	■	■		■		■	■	
	[76]	2018		■		■	■			■		■	■	
	[77]	2018			■	■	■		■			■	■	
	[78]	2019			■	■				■		■	■	
	[79]	2019			■	■	■	■		■	■		■	
	[80]	2021			■	■	■		■			■	■	
CFD	[82]	2011			■	■	■	■		■		■	■	
	[24]	2016			■	■	■	■		■		■	■	
	[50],[53],[54]	2018			■	■	■	■		■		■	■	
	[58]	2019			■	■	■	■		■		■	■	
	[85]	2020			■	■	■	■	■		■			■
	[83]	2020			■	■	■	■	■			■	■	
	[84]	2020		■		■	■	■	■		■		■	
	[85]	2020			■	■	■	■		■	■		■	
	[86]	2021			■	■	■	■	■			■	■	
	[87]	2022			■	■	■	■		■		■	■	
	[63]	2022			■	■	■	■		■		■	■	

verifying the thermal integrity, especially during converter power surges.

In most cases, a uniform loss density was applied. This hypothesis can be justified for windings owing to their high thermal conductivity. However, this hypothesis may be a source of uncertainty in the magnetic core. In addition, the possible presence of an air gap can induce a localized excess loss on the winding near it, which requires non-uniform loss modeling. Most thermal models have weak coupling. This means that the variations in the electrical and thermal properties with temperature were not considered. Hence, the nonlinearity introduced by the transformer properties and its dependency on temperature are neglected, even though they can have a significant effect on the losses and temperature values.

Finally, it can be observed from Table 4 that no model englobes all aspects of thermal modeling for the PMC. Each type of model has its own advantages and limitations, and can be used depending on the goals and requirements of the studied case. Therefore, it is important to understand the specifications of PMCs and their applications in order to apply suitable models.

To summarize, the thermal resistance model is very useful in the early design stage, but it needs to be validated by a more accurate model that cannot consider various cooling conditions. One-dimensional (1D) thermal networks are a better alternative. This is quite accurate when the component is attached to a heat sink in single- or double-sided cooling, that is, when the main heat path is from the heat sink. Otherwise, a more complex thermal network that considers 3D aspects must be used. FEA is accurate and considers 3D geometry. It can be used to study thermal management solutions, even if it is time-consuming. The use of computational fluid dynamics (CFD) is complicated and time-consuming. However, this is the most suitable method for simulating forced air and liquid cooling.

To guide designers and engineers, the next section deals with the key points for performing effective thermal modeling of the PMCs. Some critical issues that require further investigation are also discussed.

IV. KEY POINTS FOR AN ACCURATE THERMAL MODELING OF PMCs

Thermal modeling is a complex task because it involves the interactions between several elements (Fig.26). The objective of a thermal model is to estimate the temperature of a component accurately. This temperature can be a single value, such as the maximum or mean temperature, several values corresponding to temperatures in some component parts, or a temperature distribution throughout the device. Several inputs were required to compute temperature (Fig.26). The geometrical and physical properties of different parts and materials, such as the thermal conductivity, heat capacity, and emissivity, need to be determined. Therefore, the thermal environment must be specified as precisely as possible, and the losses must be accurately estimated. The latter two
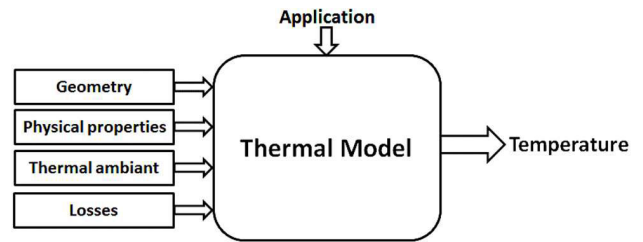

FIGURE 26. Inputs of a thermal model.

TABLE 5. PMC material maximal temperature.

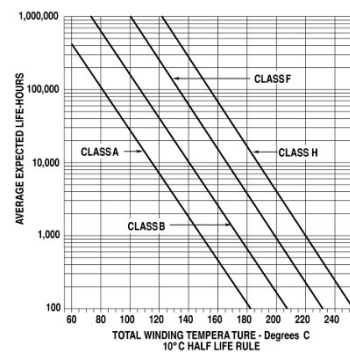| Material	Maximal operating temperature in °C
Copper	1084
Ferrite	200-250
Dielectric insulator	120-160

FIGURE 27. Cycle life example of various dielectric insulators classes [88].

elements can be functions of the working conditions and constraints specified by the application requirements.

A. FACTORS LIMITING THE OPERATING TEMPERATURE OF PMCs

Every material comprising a PMC has a temperature limit owing to its physical constraints (Table 5). Cu can operate at high temperatures, reaching hundreds of °C. Ferrite can reach a thousand of °C without melting like other ceramics. Nevertheless, its limiting point is the Curie temperature, at which ferrite loses its magnetic properties. This temperature could reach 250°C. Generally, the weakest part of the transformer is a dielectric insulator, whose maximum operating temperature is far lower than that of the other materials. Moreover, temperature has a significant impact on the insulator's expected life, as shown in Fig.27. Indeed, a 10 °C temperature increase reduces the expected life by half [88].

Table 6 presents some examples of dielectric insulator materials and their thermal classes and maximal operating temperatures according to the IEC-60085 standard [89]. For example, the maximum operating temperature of FR4, which is frequently used as an insulator in PMC PCB windings, was 120°C °C. Other insulators that can reach higher
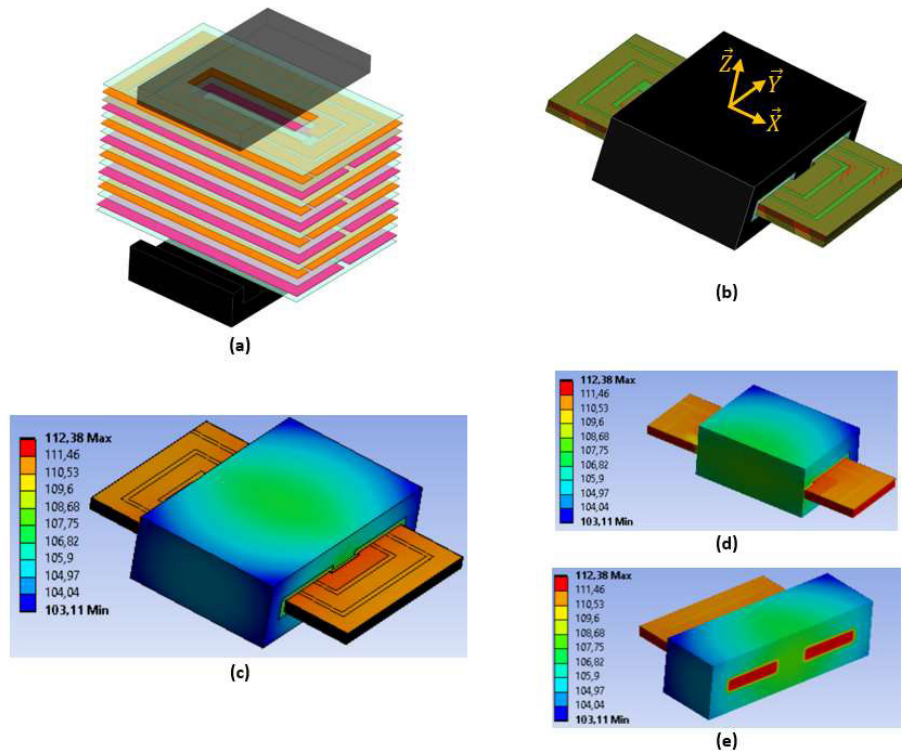
FIGURE 28. 3D FEA modeling for the parameter variation study: (a) 3D exploded view, (b) assembled planar transformer, (c) temperature distribution for nominal values, (d) internal temperature distribution (XZ plan), (e) internal temperature distribution (YZ plan).

TABLE 6. Dielectric insulators thermal classes [89].

Class	Maximal temperature °C	Examples
Y	90	Paper, cotton,silk
A	105	nylon
E	120	Terylene fibre, melinex film, polyurethanes
B	130	Mica, fiberglass, bakelite, polyster enamel, FR4
F	155	Epoxy resins
H	180	Silicone rubber, polymide film
G	255	Teflon, Kapton

temperatures can also be used for foil windings, such as Kapton. However, they are expensive and require glue, which is generally limited to the maximum operating temperature. In general, the operating temperature of planar magnetics is fixed at 100 °C. At this temperature, the core losses have a minimum value; however, for economic reasons and power density enhancement, this temperature can be increased to 130 °C.

B. PMCsTHERMAL MODELING: SOME CRITICAL ASPECTS

The thermal model computes temperature according to its input. Regarding the complexity of modeling, there are multiple sources of errors, such as losses, geometry, and boundary conditions. Hence, the computed temperature values could present large errors compared with the measured values. A simple analysis was performed based on the thermal resistance model (6). From the final equation, the relative error can be deduced as follows:

$$\frac{\Delta(\Delta T)}{\Delta T} = \frac{\Delta R_{th}}{R_{th}} + \frac{\Delta P_{loss}}{P_{loss}} \quad (16)$$

From (16), an estimation error of 10% for the losses, combined with an uncertainty of 10% for the thermal resistance, leads to a relative error of 20% in the temperature rise. Therefore, the accuracy of thermal modeling strongly depends on the accuracy of the losses and thermal resistance, which represent the boundary conditions, geometry, and materials.

To analyze the impact of the error sources, a parametric study was performed using FEA. The objective was to evaluate the impact of the material's thermal conductivities, losses, and heat exchange coefficient variation on the temperature rise. The studied planar transformer (Fig.28) is based on an E/PLT38 ferrite core and eight layers of 0.3 mm copper foil separated by a 0.1 mm Kapton insulator film. A 3D exploded view of the transformer is illustrated in Fig.28a to show the different layers and E/PLT core combination. The assembled transformer is illustrated in Fig.28b. Finally, the 3D temperature distribution resulting from the FEA is presented in Fig.28c for typical values of the planar transformer parameters (Table 7). The two cuts in the XZ and YZ plans
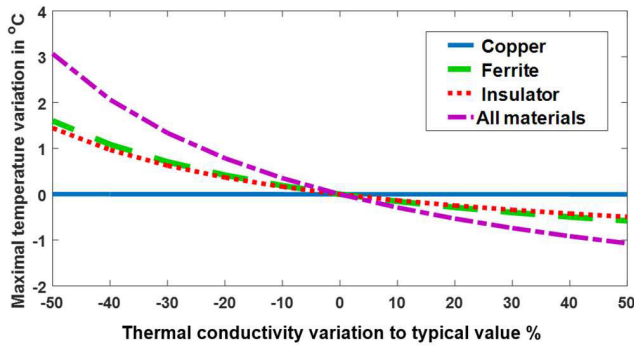
FIGURE 29. Effect of thermal conductivities on PMC temperature variation.

are presented in Fig.28d and Fig.28e, respectively, to show the internal temperature distribution.

To illustrate the impact of these parameters, the thermal conductivities (ferrite, insulator, and copper), total losses (copper + core), and heat exchange coefficient were varied in the range of ±50% from their typical values (Table 7). Fig.29 and Fig.30 show the maximal temperature variation as a function of the thermal conductivity, losses, and heat exchange coefficient, respectively. According to the results, the heat exchange coefficient and losses significantly affect the computed temperature (Fig.30). Thus, the precision of these elements must be controlled when modeling a PMC. In comparison, the thermal conductivity variations of the materials were less significant (Fig.29). A variation of 50% in all the conductivities increased the temperature by only 3 °C. Thus, these parameters were less critical.

Typically, the typical heat exchange coefficients are given by empirical formulas for various geometric configurations in free and forced convection [13], [14]. Although these formulas are useful, their accuracy is not always ensured. Only CFD simulations can accurately predict these values, particularly for complex assemblies. Fig.31 shows the evolution of the heat exchange coefficient due to convection and radiation as a function of the temperature rise of a planar transformer. These values were extracted from the CFD analysis of the same planar transformer model (Fig.28). Even if the radiation effect has been neglected by some authors (Table 4), its impact on the heat exchange coefficient can be as important as that of convection, especially for free-air-cooled components.

Even if the temperature values are affected by uncertainties, a good 3D thermal model provides a detailed temperature distribution. It can also allow access to temperature gradients and the identification of hot regions. Such a model is a useful tool for improving the thermal behavior of a design or comparing different design configurations. Moreover, an accurate thermal model can help designers to study the thermal management and cooling strategies of PMCs.

C. THERMAL MANAGEMENT OF PMCs

Natural air cooling is usually insufficient for achieving high-power-density converters. Forced air or liquid cooling was

TABLE 7. Planar transformer parameter variation.

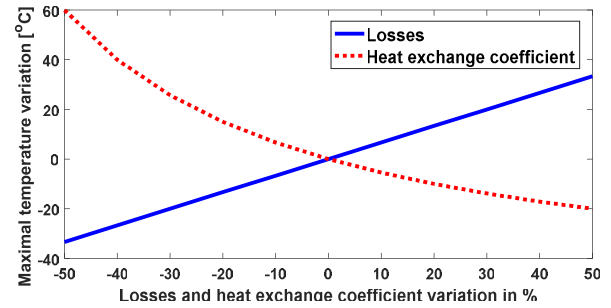| Class	Min -50%	Typical	Max +50%
Ferrite thermal conductivity [W.m^{-1}.K^{-1}]	1.75	3.5	5.25
Insulator thermal conductivity [W.m^{-1}.K^{-1}]	0.075	0.15	0.225
Copper thermal conductivity [W.m^{-1}.K^{-1}]	200	400	600
Total losses [W]	3	6	9
Heat exchange coefficient [W.m^{-2}.K^{-1}]	5	10	15

FIGURE 30. Effect of Losses and heat exchange coefficient on PMC temperature variation.
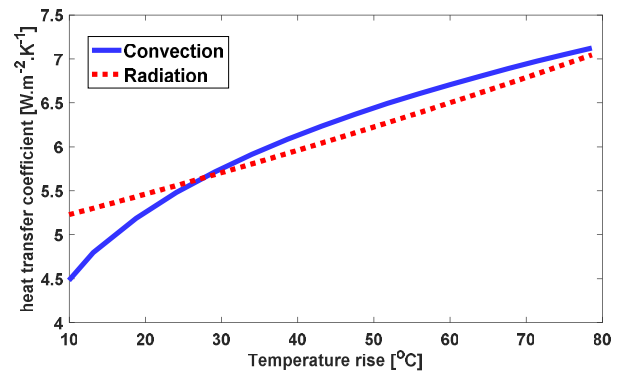

FIGURE 31. Evolution of heat exchange coefficient (convection and radiation) as a function of temperature rise.

required. However, to efficiently extract heat from the PMC, the heat path to the cooling system (e.g., item 1 in Fig.32) must be optimized. Some solutions are presented in Fig.32 to increase the heat transfer capability of the PMC. One of the most commonly used solutions is to use an aluminum cover or cap (item 2) associated with an aluminum base (item 3) surrounding the core to homogenize its temperature.

The thermal heat path shown in Fig.32 is illustrated in Fig.33. In this example, a planar component is attached to a cold plate. Without the cap and base, the main heat path was downward from the component to the cold plate, as shown in Fig.33a. With the aluminum cap (Fig.33b), the heat from the upper part and sides of the magnetic core was also canalized to the cooling system. This solution enabled a decrease in the temperature difference between the top and bottom of the core, which resulted in a more homogenous temperature and

FIGURE 32. Some solutions for thermal management and cooling of PMCs.
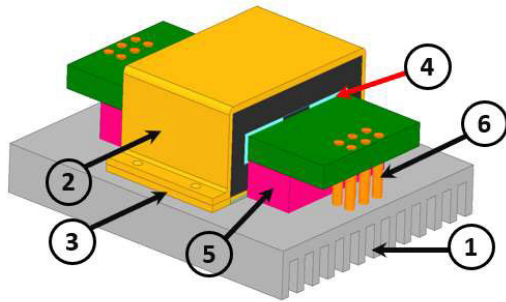
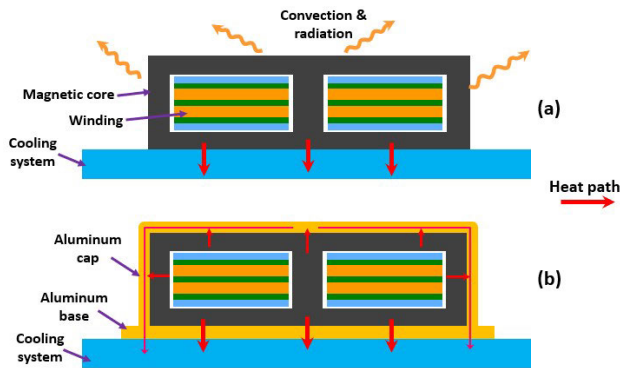| 1	Heatsink
2	Aluminium cover or cap
3	Aluminum base
4	Thermal gap filler
5	Thermal pad
6	Thermal vias

FIGURE 33. Heat path in a PMC attached to a cold plate: (a) without aluminum cap, (b) with aluminum cap and aluminum base.

ensured effective cooling. This cover also guarantees a good link between the PMC and cooling system.

If good thermal contact between the core and cooling system is implemented, it is important to have good thermal contact between the core and windings. This can be achieved by filling the core window gap with a thermal pad or glue (item 4). For high-current applications where copper losses are dominant, a thermal pad linking the winding and cooler (item 5) can be added to maximize the heat extraction from the windings. In the case of multilayer PCB windings, thermal vias (item 6) can be added to link the windings to the cooling system.

From Fig.32, extensive use of thermal interface materials can be observed. Thus, particular attention must be given to them [90], [91], [92], especially in the presence of high-temperature gradients, which is usually the case in high-power-density applications.

Thermal management must be considered during thermal modeling. This can be achieved by modeling the overall cooling system or by applying conditions such as a fixed cold plate temperature or specific exchange coefficients. For some applications, the cooling system can be studied with a
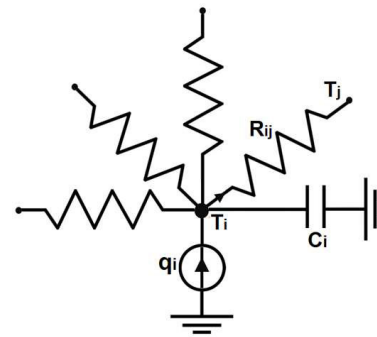

FIGURE 34. i^{th} node of the 3D thermal network [42].

separate model using an adapted tool (e.g., CFD for liquid cooling) or can be studied experimentally. This enables the designer to extract the appropriate parameters to be applied to PMC thermal modeling or to the overall power converter components.

As mentioned previously, PMCs can be cooled by free air without a heat sink or cooler. This cooling mode is the most economical; however, it does not always satisfy the thermal constraints of high-power and high-density power converters. To meet these requirements, creative methods have been developed. For example, topology optimization represents a potential interest for magnetic components.

It has been used to optimize electromagnetic aspects in several studies [93], [94], [95], [96]. Currently, it is gaining interest owing to its additive manufacturing, which makes it possible to realize complex shapes [97], [98], [99], [100] even for HF magnetics and their thermal management enhancement.

V. CONCLUSION

Planar magnetic components have been extensively used in high-density power converters. Thermal aspects have become crucial for increasing the power density.

This paper presents a review of the thermal models used in the literature. The papers were organized according to the model type and analyzed to highlight their merits and limitations. All papers were classified according to the specified criteria and analyzed.

From the analysis, it appears that thermal-resistant type models are widely used for early stage designs, owing to their simplicity. Thermal networks allow for more detailed thermal modeling and are familiar to electrical engineers. They can be very complex or compact with a reduced number of elements. One of their primary interests is compatibility with electrical simulation tools. Numerical models have been increasingly used owing to the development and accessibility of performant computers in addition to a large range of commercial and free software. Finite element modeling is the most commonly used numerical model, which provides a detailed 2D or 3D thermal distribution. CFD has started to be used, but it requires more informatic resources and time.

However, it is the best solution for studying fluid flow in air or liquid cooling.

In the last section, some issues and key points are discussed. The losses and heat exchange coefficients are critical parameters in the thermal modeling of PMCs. The accuracy of the results strongly depended on these factors. Radiation is sometimes neglected in thermal modeling, and it has been shown that its effect can be similar to that of convection.

Thermal modeling, especially 3D modeling, will be extensively used in the future, particularly to study complex shapes linked to new thermal management methods or emerging topology optimization and additive manufacturing concepts.

APPENDIX A
To solve the model presented in Fig.10c, vectors and matrix are defined. Node temperatures are grouped in a temperature vector denoted by T (17). The losses and known temperatures at the boundaries of the model (T_{10} and T_{20}) were set in another vector, P (18). Finally, an admittance matrix A is introduced to link the two vectors in (19), as shown at the bottom of the page.

$$T = \begin{pmatrix} T_1 \\ T_2 \\ \vdots \\ T_{N+1} \end{pmatrix} \qquad (17)$$

$$P = \begin{pmatrix} T_{10} \\ P_{core\_1} \\ P_{Cu\_1} \\ \vdots \\ P_{Cu\_n} \\ P_{core\_2} \\ T_{20} \end{pmatrix} \qquad (18)$$

The temperature vector can be computed by:

$$T = A^{-1}P \qquad (20)$$

To establish the model, the thermal resistance of the ith layer is given by

$$R_{thi} = \frac{L_i}{S.k_i} \qquad (21)$$

where L_i is the ith layer thickness, S is the layer section, and k_i is the ith layer's thermal conductivity.

The thermal resistances modeling the heat exchange with exterior can be computed by:

$$R_{th} = \frac{1}{S.h_{ex}} \qquad (22)$$

where h_{ex} is the heat exchange coefficient and S is the exchange surface

APPENDIX B
The model introduced in [42] can be derived from Kirchoff's laws applied to the ith node of the thermal resistance network, as illustrated in Fig.34:

$$\sum_{j=1}^{n} \frac{T_i - T_j}{R_{ij}} - q_i = C_i \frac{dT_i}{dt} \qquad (23)$$

The thermal network contains n nodes. From (23), the node temperatures are split into 1 to m with unknown temperatures, and m+1 to n with known temperatures:

$$\left(\sum_{j=1}^{n} \frac{1}{R_{ij}} \right) T_i - \sum_{j=1}^{m} \frac{1}{R_{ij}} T_j - \sum_{j=m+1}^{n} \frac{1}{R_{ij}} T_j + q_i = C_i \frac{dT_i}{dt} \qquad (24)$$

Equation (24) is rewritten with admittances G_{ij}:

$$\left(\sum_{j=1}^{n} G_{ij} \right).T_i - \sum_{j=1}^{m} G_{ij}.T_j - \sum_{j=m+1}^{n} G_{ij}.T_j + q_i = C_i \frac{dT_i}{dt} \qquad (25)$$

where $G_{ij} = \frac{1}{R_{ij}}$

Finally, the problem is set under matrix form:

$$AT - BU = 0 \qquad (26)$$

$$A = \begin{pmatrix} 1 & 0 & 0 & 0 & \cdots & 0 & 0 & 0 \\ \frac{-1}{R_{th1}} & \frac{1}{R_{th1}} + \frac{1}{R_{th2}} & \frac{-1}{R_{th2}} & 0 & \cdots & 0 & 0 & 0 \\ 0 & \frac{-1}{R_{th2}} & \frac{1}{R_{th2}} + \frac{1}{R_{th3}} & \frac{-1}{R_{th3}} & \cdots & 0 & 0 & 0 \\ \vdots & \vdots & \ddots & \ddots & \vdots & \vdots & \vdots & \vdots \\ 0 & 0 & \cdots & 0 & \frac{-1}{R_{thN-1}} & \frac{1}{R_{thN-1}} + \frac{1}{R_{thN}} & \frac{-1}{R_{thN}} & 0 \\ 0 & 0 & \cdots & 0 & 0 & 0 & 0 & 1 \end{pmatrix} \qquad (19)$$

$$B = \begin{pmatrix} 1 & 0 & \ldots & 0 & -G_{1(m+1)} & -G_{1(m+2)} & \ldots & -G_{1n} \\ 0 & 1 & \ldots & 0 & -G_{2(m+1)} & -G_{2(m+2)} & \ldots & -G_{1n} \\ \vdots & \vdots & \ddots & \vdots & \vdots & \vdots & \ldots & \vdots \\ 0 & 0 & \ldots & 1 & -G_{m(m+1)} & -G_{m(m+2)} & \ldots & -G_{mn} \end{pmatrix} \qquad (28)$$

where A admittance matrix (27), B is the known temperature vector (28), as shown at the bottom of the previous page, and T is an unknown temperature vector.

$$A = \begin{pmatrix} \sum_{j=1}^{n} G_{1j} & -G_{12} & \cdots & -G_{1m} \\ -G_{21} & \sum_{j=1}^{n} G_{2j} & \cdots & -G_{2m} \\ \vdots & \vdots & \ddots & \vdots \\ -G_{1m} & -G_{2m} & \ldots & \sum_{j=1}^{n} G_{mj} \end{pmatrix} \quad (27)$$

Finally, temperature can be computed by:

$$T = A^{-1}BU \quad (29)$$

REFERENCES

[1] G. Di Capua, N. Femia, and K. Stoyka, "Power magnetics volume and weight reduction in aerospace power supply units," in *Proc. IEEE 17th Workshop Control Modeling Power Electron. (COMPEL)*, Jun. 2016, pp. 1–6, doi: 10.1109/COMPEL.2016.7556728.

[2] J. W. Kolar, U. Drofenik, J. Biela, M. L. Heldwein, H. Ertl, T. Friedli, and S. D. Round, "PWM converter power density barriers," in *Proc. Power Convers. Conf.*, Apr. 2007, pp. 9–29, doi: 10.1109/PCCON.2007.372914.

[3] J. Millan, P. Godignon, X. Perpina, A. Perez-Tomas, and J. Rebollo, "A survey of wide bandgap power semiconductor devices," *IEEE Trans. Power Electron.*, vol. 29, no. 5, pp. 2155–2163, May 2014, doi: 10.1109/TPEL.2013.2268900.

[4] X. She, A. Q. Huang, Ó. Lucía, and B. Ozpineci, "Review of silicon carbide power devices and their applications," *IEEE Trans. Ind. Electron.*, vol. 64, no. 10, pp. 8193–8205, Oct. 2017, doi: 10.1109/TIE.2017.2652401.

[5] A. Hassan, Y. Savaria, and M. Sawan, "GaN integration technology, an ideal candidate for high-temperature applications: A review," *IEEE Access*, vol. 6, pp. 78790–78802, 2018, doi: 10.1109/ACCESS.2018.2885285.

[6] R. Sun, J. Lai, W. Chen, and B. Zhang, "GaN power integration for high frequency and high efficiency power applications: A review," *IEEE Access*, vol. 8, pp. 15529–15542, 2020, doi: 10.1109/ACCESS.2020.2967027.

[7] G. Iannaccone, C. Sbrana, I. Morelli, and S. Strangio, "Power electronics based on wide-bandgap semiconductors: Opportunities and challenges," *IEEE Access*, vol. 9, pp. 139446–139456, 2021, doi: 10.1109/ACCESS.2021.3118897.

[8] M. Parvez, A. T. Pereira, N. Ertugrul, N. H. E. Weste, D. Abbott, and S. F. Al-Sarawi, "Wide bandgap DC–DC converter topologies for power applications," *Proc. IEEE*, vol. 109, no. 7, pp. 1253–1275, Jul. 2021, doi: 10.1109/JPROC.2021.3072170.

[9] Z. Ouyang and M. A. E. Andersen, "Overview of planar magnetic technology—Fundamental properties," *IEEE Trans. Power Electron.*, vol. 29, no. 9, pp. 4888–4900, Sep. 2014, doi: 10.1109/TPEL.2013.2283263.

[10] J. S. N. T. Magambo, R. Bakri, X. Margueron, P. Le Moigne, A. Mahe, S. Guguen, and T. Bensalah, "Planar magnetic components in more electric aircraft: Review of technology and key parameters for DC–DC power electronic converter," *IEEE Trans. Transport. Electrific.*, vol. 3, no. 4, pp. 831–842, Dec. 2017, doi: 10.1109/TTE.2017.2686327.

[11] A. Estrov, "Transformer design for 1 MHz resonant converter," Tech. Rep., 1986.

[12] M. T. Quirke, J. J. Barrett, and M. Hayes, "Planar magnetic component technology—A review," *IEEE Trans. Compon., Hybrids, Manuf. Technol.*, vol. 15, no. 5, pp. 884–892, Oct. 1992, doi: 10.1109/33.180055.

[13] A. Bejan and A. D. Kraus, *Heat Transfer Handbook*. Hoboken, NJ, USA: Wiley, 2003.

[14] R. H. Pletcher, J. C. Tannehill, and D. A. Anderson, *Computational Fluid Mechanics and Heat Transfer*. Boca Raton, FL, USA: CRC Press, 2013.

[15] F. P. Incropera, D. P. DeWitt, T. L. Bergman, and A. S. Lavine, *Principles of Heat and Mass Transfer*, 7th ed. Singapore: Wiley, 2013.

[16] *Design of Planar Power Transformers*, Ferroxcube, Dongguan, China, 1997.

[17] *Ferroxcube Soft Ferrites Design Tool (SFDT)*. Accessed: Mar. 29, 2021. [Online]. Available: https://www.ferroxcube.com/en-global/design_tool/index

[18] W. G. Hurley and W. H. Wölfle, *Transformers and Inductors for Power Electronics: Theory, Design and Applications*. Chichester, West Sussex: Wiley, 2013.

[19] W. J. Muldoon, "Analytical design optimization of electronic power transformers," in *Proc. IEEE Power Electron. Spec. Conf.*, Jun. 1978, pp. 216–225, doi: 10.1109/PESC.1978.7072356.

[20] *Magnetics Designer—Personal Computer Circuit Design Tools*. Accessed: Mar. 29, 2021. [Online]. Available: http://www.intusoft.com/lit/Magdes.pdf

[21] A. van den Bossche and V. Valchev. (2005). *Inductors and Transformers for Power Electronics*. Accessed: Nov. 25, 2020. [Online]. Available: https://www.taylorfrancis.com/books/e/9781420027280

[22] C. W. T. McLyman, *Transformer and Inductor Design Handbook*. New York, NY, USA: M. Dekker, 1978.

[23] Z. Zhang and K. D. T. Ngo, "Multi-megahertz quasi-square-wave flyback converter using eGaN FETs," *IET Power Electron.*, vol. 10, no. 10, pp. 1138–1146, Aug. 2017, doi: 10.1049/iet-pel.2016.0782.

[24] R. Bakri, J. S. N. Teu, X. Margueron, P. Le Moigne, and N. Idir, "Planar transformer equivalent thermal resistance variation with ambient temperature and power losses," in *Proc. 18th Eur. Conf. Power Electron. Appl.*, Sep. 2016, pp. 1–9, doi: 10.1109/EPE.2016.7695431.

[25] M. P. Sayani, G. R. Skutt, and P. S. Venkatraman, "Electrical and thermal performance of PWB transformers," in *Proc. 6th Annu. Appl. Power Electron. Conf. Exhib.*, Mar. 1991, pp. 533–542, doi: 10.1109/APEC.1991.146229.

[26] R. Chen, F. Canales, B. Yang, and J. D. van Wyk, "Volumetric optimal design of passive integrated power electronics module (IPEM) for distributed power system (DPS) front-end DC/DC converter," *IEEE Trans. Ind. Appl.*, vol. 41, no. 1, pp. 9–17, Jan. 2005, doi: 10.1109/TIA.2004.841026.

[27] D. van der Linde, C. A. M. Boon, and J. B. Klaassens, "Design of a high-frequency planar power transformer in multilayer technology," *IEEE Trans. Ind. Electron.*, vol. 38, no. 2, pp. 135–141, Apr. 1991, doi: 10.1109/41.88907.

[28] M. C. Smit, J. A. Ferreira, J. D. van Wyk, and M. Ehsani, "Technology for manufacture of integrated planar LC structures for power electronic applications," in *Proc. 5th Eur. Conf. Power Electron. Appl.*, Sep. 1993, pp. 173–178.

[29] L. M. Escribano, R. Prieto, J. A. Oliver, J. A. Cobos, and J. Uceda, "Analytical model for magnetic components including self-heating effects," in *Proc. IEEE 35th Annu. Power Electron. Spec. Conf.*, Jun. 2004, pp. 867–872, doi: 10.1109/PESC.2004.1355532.

[30] Y. Park, S. Yuruker, S. Chakraborty, A. Khaligh, R. Mandel, P. McCluskey, M. Ohadi, L. Boteler, and M. Hinojosa, "Electro-thermal co-design of a cooling system-integrated high-frequency transformer," in *Proc. IEEE Transp. Electrific. Conf. Expo (ITEC)*, Jun. 2020, pp. 26–31, doi: 10.1109/ITEC48692.2020.9161660.

[31] L. M. Escribano, R. Prieto, J. A. Oliver, and J. A. Cobos, "A new approach to obtain 1D thermal models for magnetic components including the effect of spacing between conductors," in *Proc. 21st Annu. IEEE Appl. Power Electron. Conf. Expo.*, Apr. 2006, p. 6, doi: 10.1109/APEC.2006.1620598.

[32] *PSPICE Software*. [Online]. Available: https://www.pspice.com/

[33] *PSIM Software*. [Online]. Available: https://powersimtech.com/products/psim/capabilities-applications/

[34] *Saber Software*. [Online]. Available: https://www.synopsys.com/verification/virtual-prototyping/saber.html

[35] *LTSPICE Software*. [Online]. Available: https://www.analog.com/en/design-center/design-tools-and-calculators/ltspice-simulator.html#

[36] A. Lewaiter and B. Ackermann, "A thermal model for planar transformers," in *Proc. 4th IEEE Int. Conf. Power Electron. Drive Syst.*, Oct. 2001, pp. 669–673, doi: 10.1109/PEDS.2001.975399.

[37] Z. Belkaid, P. Enrici, F. Forest, T. Martire, and J.-J. Huselstein, "Development of models and tool for the design of HF magnetic components in power electronics," in *Proc. IEEE Int. Conf. Ind. Technol. (ICIT)*, Feb. 2018, pp. 706–711, doi: 10.1109/ICIT.2018.8352264.

[38] *COMSOL Multiphysics Software*. Accessed: Mar. 30, 2021. [Online]. Available: https://www.comsol.com/

[39] K. Lai-Dac, Y. Lembeye, and B. Sarrazin, "Two free air convection and radiation thermal models for planar magnetic components," in *Proc. IEEE Int. Symp. Ind. Electron.*, Jun. 2011, pp. 456–461, doi: 10.1109/ISIE.2011.5984068.

[40] R. Shafaei, M. Ordonez, and M. A. Saket, "Three-dimensional frequency-dependent thermal model for planar transformers in LLC resonant converters," *IEEE Trans. Power Electron.*, vol. 34, no. 5, pp. 4641–4655, May 2019, doi: 10.1109/TPEL.2018.2859839.

[41] *Flux: Software for Electromagnetic Methods Simulation*. [Online]. Available: https://www.altair.com/flux/

[42] R. Bakri, X. Margueron, J. S. N. T. Magambo, P. Le Moigne, and N. Idir, "Automated tool for 3D planar magnetic temperature modelling: Application to EE and E/PLT core-based components," *IET Power Electron.*, vol. 12, no. 15, pp. 4043–4053, Dec. 2019, doi: 10.1049/iet-pel.2019.0332.

[43] Y. Gao, V. Sankaranarayanan, E. M. Dede, Y. Zhou, F. Zhou, R. W. Erickson, and D. Maksimovic, "Modeling and design of high-power, high-current-ripple planar inductors," *IEEE Trans. Power Electron.*, vol. 37, no. 5, pp. 5816–5832, May 2022, doi: 10.1109/TPEL.2021.3132563.

[44] H. Pape and G. Noebauer, "Generation and verification of boundary independent compact thermal models for active components according to the DELPHI/SEED methods," in *Proc. 15th Annu. IEEE Semiconductor Thermal Meas. Manage. Symp.*, Mar. 1999, pp. 201–211, doi: 10.1109/STHERM.1999.762449.

[45] M.-N. Sabry, "Compact thermal models for electronic systems," *IEEE Trans. Compon. Packag. Technol.*, vol. 26, no. 1, pp. 179–185, Mar. 2003, doi: 10.1109/TCAPT.2002.808009.

[46] M. Rascon, J. Ara, R. Madsen, J. Navas, M. Perez, and F. San Miguel, "Thermal analysis and modelling of planar magnetic components," in *Proc. 16th Annu. IEEE Appl. Power Electron. Conf. Expo.*, Mar. 2001, pp. 97–101, doi: 10.1109/APEC.2001.911633.

[47] *Pyton Planar Magnetics*. [Online]. Available: https://www.paytongroup.com

[48] *Standex Electronics*. [Online]. Available: https://standexelectronics.com/products/planar-magnetics/

[49] *Coilcraft*. [Online]. Available: https://www.coilcraft.com/

[50] V. Bissuel, E. Monier-Vinard, A. Olivier, B. Rogie, A. Mahe, N. Laraqi, and C. Gougis, "Investigation of DELPHI-inspired compact thermal model for modeling planar transformer—Network concept," in *Proc. 19th Int. Conf. Thermal, Mech. Multi-Phys. Simulation Exp. Microelectron. Microsyst.)*, Apr. 2018, pp. 1–10, doi: 10.1109/EuroSimE.2018.8369907.

[51] K. Gorecki and K. Gorski, "Compact thermal model of planar transformers," in *Proc. 24th Int. Conf. 'Mixed Design Integr. Circuits Syst.'*, Jun. 2017, pp. 345–350, doi: 10.23919/MIXDES.2017.8005229.

[52] A. Strong, "JEDEC overview," in *Proc. IEEE Int. Integr. Rel. Workshop Final Rep.*, Oct. 2008, p. 145, doi: 10.1109/IRWS.2008.4796109.

[53] *Using the Delphi Method|IEEE Conference Publication|IEEE Xplore*. Accessed: Dec. 1, 2021. [Online]. Available: https://ieeexplore.ieee.org/document/6017716

[54] V. Bissuel, L. Codecasa, E. Monier-Vinard, B. Rogié, A. Olivier, A. Mahé, N. Laraqi, V. Alessandro, and C. Gougis, "Novel approach to the extraction of Delphi-like boundary-condition-independent compact thermal models of planar transformer devices," in *Proc. 24rd Int. Workshop Thermal Investigations ICs Syst. (THERMINIC)*, Sep. 2018, pp. 1–7, doi: 10.1109/THERMINIC.2018.8593283.

[55] V. Bissuel, E. Monier-Vinard, L. Codecasa, N.-M. Nguyen, A. Mahe, O. Daniel, N. Laraqi, and V. D'Alessandro, "Practical thermal modeling of planar magnetic component devices," in *Proc. 18th IEEE Intersoc. Conf. Thermal Thermomech. Phenomena Electron. Syst. (ITherm)*, May 2019, pp. 745–754, doi: 10.1109/ITHERM.2019.8757289.

[56] M. Akbari, M. Tavakoli Bina, A. S. Bahman, B. Eskandari, E. Pouresmaeil, and F. Blaabjerg, "An extended multilayer thermal model for multichip IGBT modules considering thermal aging," *IEEE Access*, vol. 9, pp. 84217–84230, 2021, doi: 10.1109/ACCESS.2021.3083063.

[57] K. Górecki and J. Zarębski, "Modeling the influence of selected factors on thermal resistance of semiconductor devices," *IEEE Trans. Compon., Packag., Manuf. Technol.*, vol. 4, no. 3, pp. 421–428, Mar. 2014, doi: 10.1109/TCPMT.2013.2290743.

[58] Z. Shen, Y. Shen, and H. Wang, "Thermal modelling of planar transformers considering internal power loss distribution," in *Proc. IEEE 4th Int. Future Energy Electron. Conf. (IFEEC)*, Nov. 2019, pp. 1–5, doi: 10.1109/IFEEC47410.2019.9015030.

[59] K. Gorecki and K. Gorski, "Non-linear thermal model of planar transformers," in *Proc. 21st Eur. Microelectron. Packag. Conf. (EMPC) Exhib.*, Sep. 2017, pp. 1–5, doi: 10.23919/EMPC.2017.8346913.

[60] K. Górecki, K. Detka, and K. Górski, "Compact thermal model of the pulse transformer taking into account nonlinearity of heat transfer," *Energies*, vol. 13, no. 11, p. 2766, Jun. 2020, doi: 10.3390/en13112766.

[61] K. Górecki and J. Zarębski, "Nonlinear compact thermal model of power semiconductor devices," *IEEE Trans. Compon., Packag. Technol.*, vol. 33, no. 3, pp. 643–647, Sep. 2010, doi: 10.1109/TCAPT.2010.2052052.

[62] Z. Shen, Y. Shen, B. Liu, and H. Wang, "Thermal coupling and network modeling for planar transformers," in *Proc. IEEE Energy Convers. Congr. Expo. (ECCE)*, Sep. 2018, pp. 3527–3533, doi: 10.1109/ECCE.2018.8558235.

[63] Z. Shen, B. Xu, C. Liu, C. Hu, B. Liu, Z. Xu, L. Jin, and W. Chen, "The modeling and simplification of a thermal model of a planar transformer based on internal power loss," *Sustainability*, vol. 14, no. 19, p. 11915, Sep. 2022, doi: 10.3390/su141911915.

[64] C. Buccella, C. Cecati, and F. de Monte, "A computational method of temperature distribution in high frequency planar transformers," in *Proc. IEEE Int. Symp. Ind. Electron.*, Jun. 2011, pp. 477–482, doi: 10.1109/ISIE.2011.5984072.

[65] C. Buccella, C. Cecati, and F. D. Monte, "A coupled electrothermal model for planar transformer temperature distribution computation," *IEEE Trans. Ind. Electron.*, vol. 55, no. 10, pp. 3583–3590, Oct. 2008, doi: 10.1109/TIE.2008.2003102.

[66] *ANSYS—Simulation Driven Product Development*. [Online]. Available: http://www.ansys.com, Accessed: Mar. 30, 2021.

[67] P. Svasta, C. Ionescu, N.-D. Codreanu, and V. Golumbeanu, "Thermal characterisation of planar transformers," in *Proc. 27th Int. Spring Seminar Electron. Technol., Meeting Challenges Electron. Technol. Prog.*, May 2004, pp. 280–286, doi: 10.1109/ISSE.2004.1490435.

[68] M. Gerber, J. A. Ferreira, I. W. Hofsajer, and N. Seliger, "A high-density heat-sink-mounted inductor for automotive applications," *IEEE Trans. Ind. Appl.*, vol. 40, no. 4, pp. 1031–1038, Jul. 2004, doi: 10.1109/TIA.2004.830766.

[69] M. Bernardoni, N. Delmonte, P. Cova, and R. Menozzi, "Thermal modeling of planar transformer for switching power converters," *Microelectron. Rel.*, vol. 50, nos. 9–11, pp. 1778–1782, Sep. 2010, doi: 10.1016/j.microrel.2010.07.129.

[70] R. Wrobel, A. Mlot, and P. H. Mellor, "Contribution of end-winding proximity losses to temperature variation in electromagnetic devices," *IEEE Trans. Ind. Electron.*, vol. 59, no. 2, pp. 848–857, Feb. 2012, doi: 10.1109/TIE.2011.2148686.

[71] L. A. R. Tria, D. Zhang, and J. E. Fletcher, "Electromagnetic and thermal characterisation of PCB planar transformer," in *Proc. IEEE 11th Int. Conf. Power Electron. Drive Syst.*, Jun. 2015, pp. 1024–1028, doi: 10.1109/PEDS.2015.7203512.

[72] *Institute of Printed Circuits, IPC-2152 Standard for Determining Current Carrying Capacity in Printed Board Design*, Standard IPC-2152, Bannockburn, 2009.

[73] C. Ropoteanu, N.-D. Codreanu, and C. Ionescu, "Thermal investigation of a planar core power transformer," in *Proc. 39th Int. Spring Seminar Electron. Technol. (ISSE)*, May 2016, pp. 112–115, doi: 10.1109/ISSE.2016.7563171.

[74] C. Ropoteanu, P. Svasta, and I. Busu, "High-frequency power loss investigation of a planar ferrite core transformer," in *Proc. IEEE 21st Int. Symp. Design Technol. Electron. Packag. (SIITME)*, Oct. 2015, pp. 61–64, doi: 10.1109/SIITME.2015.7342296.

[75] C. Ropoteanu, P. Svasta, and C. Ionescu, "Electro-thermal simulation study of different core shape planar transformer," in *Proc. IEEE 22nd Int. Symp. Design Technol. Electron. Packag. (SIITME)*, Oct. 2016, pp. 209–212, doi: 10.1109/SIITME.2016.7777279.

[76] B. Rao, Y. Zhao, Y. Yang, J. Gao, Z. Zhang, S. Zhou, M. Zhang, and Z. Chen, "Reduction of leakage inductance and AC resistance of planar transformers by optimising the current distribution," *IET Power Electron.*, vol. 11, no. 3, pp. 501–506, Mar. 2018, doi: 10.1049/iet-pel.2017.0362.

[77] R. Shafaei, M. A. Saket, and M. Ordonez, "Thermal comparison of planar versus conventional transformers used in LLC resonant converters," in *Proc. IEEE Energy Convers. Congr. Expo. (ECCE)*, Sep. 2018, pp. 5081–5086, doi: 10.1109/ECCE.2018.8557894.

[78] G. Salinas, J. A. Oliver, J. Munoz-Anton, A. Fernandez, and R. Prieto, "Thermal management of planar magnetics for spacecrafts: Characterization and modeling," in *Proc. Eur. Space Power Conf. (ESPC)*, Sep. 2019, pp. 1–6, doi: 10.1109/ESPC.2019.8932068.

[79] C. Winter, J. Riedel, and S. Butzmann, "Improved heat dissipation through copper bricks for high turns ratio planar transformers," in *Proc. 20th Int. Symp. Power Electron. (EE)*, Oct. 2019, pp. 1–6, doi: 10.1109/PEE.2019.8923546.

[80] E. M. Dede, Y. Gao, Y. Zhou, V. Sankaranarayanan, F. Zhou, D. Maksimovic, and R. W. Erickson, "Thermal design, optimization, and packaging of planar magnetic components," *IEEE Trans. Compon., Packag., Manuf. Technol.*, vol. 11, no. 9, pp. 1480–1488, Sep. 2021, doi: 10.1109/TCPMT.2021.3105003.

[81] Z. Yu, X. Yang, G. Wei, L. Wang, K. Wang, W. Chen, and J. Wei, "A novel high-current planar inductor with cooling fins based on 3-D printing," *IEEE Trans. Power Electron.*, vol. 36, no. 11, pp. 12189–12195, Nov. 2021, doi: 10.1109/TPEL.2021.3078083.

[82] W. Lu and G. Chunying, "Detailed design of high-frequency planar power transformer," in *Proc. 6th IEEE Conf. Ind. Electron. Appl.*, Jun. 2011, pp. 1610–1614, doi: 10.1109/ICIEA.2011.5975848.

[83] A. L. Ganga, S. Reyhan, R. Re, J.-M. Dalbavie, and P. Guglielmi, "Losses and thermal considerations on an IPOS structure with 20 kW high-frequency planar transformers," in *Proc. Int. Conf. Electr. Mach. (ICEM)*, Aug. 2020, pp. 921–926, doi: 10.1109/ICEM49940.2020.9270944.

[84] Z. Zhang, C. Liu, M. Wang, Y. Si, Y. Liu, and Q. Lei, "High-efficiency high-power-density CLLC resonant converter with low-stray-capacitance and well-heat-dissipated planar transformer for EV on-board charger," *IEEE Trans. Power Electron.*, vol. 35, no. 10, pp. 10831–10851, Oct. 2020, doi: 10.1109/TPEL.2020.2980313.

[85] M. A. Kolobov, A. V. Okunev, and D. V. Bushmanov, "Research of planar transformer properties using Ansys software," in *Proc. Int. Conf. Ind. Eng., Appl. Manuf. (ICIEAM)*, May 2020, pp. 1–5, doi: 10.1109/ICIEAM48468.2020.9111980.

[86] M. Ngo, Y. Cao, K. Nguyen, D. Dong, and R. Burgos, "Computational fluid dynamic analysis and design of an air duct cooling system for 18 kW, 500 kHz planar transformers," in *Proc. IEEE Appl. Power Electron. Conf. Exposit. (APEC)*, Jun. 2021, pp. 1496–1504, doi: 10.1109/APEC42165.2021.9487172.

[87] J. Köhler Mendizábal, M. Montazeri, D. Huitink, and N. Miljkovic, "Direct cooling of a planar magnetic converter using dielectric liquid forced convection enabled by additive manufacturing," *Int. J. Heat Mass Transf.*, vol. 191, Aug. 2022, Art. no. 122809, doi: 10.1016/j.ijheatmasstransfer.2022.122809.

[88] *IEEE Standard Test Procedure for Thermal Evaluation of Systems of Insulating Materials for Random-Wound AC Electric Machinery*, IEEE Standard 117-2015, May 2016, doi: 10.1109/IEEESTD.2016.7466454.

[89] *International Standard: Electrical Insulation—Thermal Evaluation and Designation*, Standard IEC-600852007, 2007.

[90] S. Chen and N.-C. Lee, "High performance thermal interface materials with enhanced reliability," in *Proc. 28th Annu. IEEE Semiconductor Thermal Meas. Manage. Symp. (SEMI-THERM)*, Mar. 2012, pp. 348–353, doi: 10.1109/STHERM.2012.6188872.

[91] P. Rodgers, V. Eveloy, E. Rahim, and D. Morgan, "Thermal performance and reliability of thermal interface materials: A review," in *Proc. 7th Int. Conf. Thermal, Mech. Multiphys. Simulation Exp. Micro-Electron. Micro-Syst.*, Apr. 2006, pp. 1–2, doi: 10.1109/ESIME.2006.1644070.

[92] J. Hansson, C. Zanden, L. Ye, and J. Liu, "Review of current progress of thermal interface materials for electronics thermal management applications," in *Proc. IEEE 16th Int. Conf. Nanotechnol. (IEEE-NANO)*, Aug. 2016, pp. 371–374, doi: 10.1109/NANO.2016.7751383.

[93] K. H. Lee, K. S. Seo, H. S. Choi, and I. H. Park, "Multiple level set method for multi-material shape optimization in electromagnetic system," *Int. J. Appl. Electromagn. Mech.*, vol. 56, pp. 183–193, Feb. 2018, doi: 10.3233/JAE-172290.

[94] Y. Otomo and H. Igarashi, "3-D topology optimization of magnetic cores for wireless power transfer with double-sided winding coils," *Int. J. Appl. Electromagn. Mech.*, vol. 60, pp. S115–S123, May 2019, doi: 10.3233/JAE-191110.

[95] T. Pham, P. Kwon, and S. Foster, "Additive manufacturing and topology optimization of magnetic materials for electrical machines—A review," *Energies*, vol. 14, no. 2, p. 283, Jan. 2021, doi: 10.3390/en14020283.

[96] C. Huber, M. Goertler, C. Abert, F. Bruckner, M. Groenefeld, I. Teliban, and D. Suess, "Additive manufactured and topology optimized passive shimming elements for permanent magnetic systems," *Sci. Rep.*, vol. 8, no. 1, p. 14651, Oct. 2018, doi: 10.1038/s41598-018-33059-w.

[97] Y. Yan, J. Moss, K. D. T. Ngo, Y. Mei, and G.-Q. Lu, "Additive manufacturing of toroid inductor for power electronics applications," *IEEE Trans. Ind. Appl.*, vol. 53, no. 6, pp. 5709–5714, Nov. 2017, doi: 10.1109/TIA.2017.2729504.

[98] C. Ding, S. Lu, J. Moss, J. Mullenix, Y. Mei, K. D. T. Ngo, and G.-Q. Lu, "Additive manufacturing of spiral windings for a pot-core constant-flux inductor," *IEEE J. Emerg. Sel. Topics Power Electron.*, vol. 8, no. 1, pp. 618–625, Mar. 2020, doi: 10.1109/JESTPE.2019.2934355.

[99] R. Wrobel and B. Mecrow, "A comprehensive review of additive manufacturing in construction of electrical machines," *IEEE Trans. Energy Convers.*, vol. 35, no. 2, pp. 1054–1064, Jun. 2020, doi: 10.1109/TEC.2020.2964942.

[100] C. Ding, S. Lu, L. Liu, K. D. T. Ngo, and G.-Q. Lu, "Additive manufacturing of hetero-magnetic coupled inductors," *IEEE Trans. Compon., Packag., Manuf. Technol.*, vol. 11, no. 6, pp. 1028–1034, Jun. 2021, doi: 10.1109/TCPMT.2021.3083179.

REDA BAKRI was born in Bouizakarne, Morocco, in 1988. He received the Engineering and master's degrees in electrical engineering for sustainable development from Ecole Nationale Superieure des Arts et Metiers (ENSAM), Lille, France, in 2014. He is currently a Researcher with Centrale Lille Institute, Villeneuve d'Ascq, France. His research interests include high-frequency and high-power-density integrated magnetic electro-thermal modeling, design and optimization, and the electro-thermal modeling of batteries for electric vehicles.
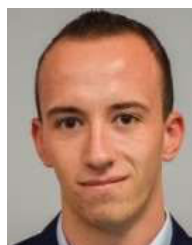
GAUTIER CORGNE was born in Sedan, France, in 1998. He received the Engineering degree and the master's degree in electrical engineering for sustainable development from Centrale Lille Institut—École Centrale de Lille, Lille, France, in 2022 and 2022, respectively. He is currently a certified teacher in engineering sciences–electrical engineering–in secondary school. His research interests include HF magnetics modeling and design for electrical mobility applications.

XAVIER MARGUERON (Member, IEEE) was born in Chambery, France, in 1980. He received the Engineering degree in electrical engineering from Ecole Nationale Superieure d'Ingenieurs Electriciens de Grenoble, Saint Martin d'Heres, France, in 2003, and the Ph.D. degree in electrical engineering from Universite Joseph Fourier, Grenoble, France, in 2006. Since 2007, he has been an Associate Professor with Centrale Lille, Villeneuve d'Ascq, France, where he has conducted research with the L2EP Laboratory. His current research interests include the modeling and optimization of HF magnetic passive components for power electronic converters and planar magnetic technology.

• • •